Electromagnetically Induced Transparency and Light Storage in Optically Dense Atomic Vapour

Gunnar Langfahl-Klabes,
Worcester College, Oxford

Submitted for the degree of Doctor of Philosophy
Feb 2015

Supervised by
Dr. Axel Kuhn

Clarendon Laboratory
University of Oxford
United Kingdom

Electromagnetically induced transparency and light storage in optically dense atomic vapour

Abstract

This thesis set out to investigate light storage based on dynamic electromagnetically induced transparency (EIT) in a room-temperature atomic ensemble of rubidium as a means to provide a quantum memory for single-photons created by a single rubidium atom coupled to a high-finesse optical resonator.

Setting up the light storage medium presented a new addition to the research group's portfolio of experimental techniques and led to investigations of EIT, slow light and stored light in warm rubidium-87 vapour. Lambda level schemes connecting Zeeman or hyperfine substates on the D_1 and D_2 lines were addressed in rubidium vapour cells containing different buffer gases and different isotopic fractions of rubidium-87 and rubidium-85.

Single beam spectroscopy with a weak probe was used to characterise the vapour cells. A numerical method to fit the D line spectrum to a theoretical model to include isotopic fractions and collisional broadening of a buffer gas has been implemented. Temperature and isotopic fractions could be reliably extracted from the fit parameters.

For an offset-stabilisation of two lasers to address a lambda level scheme connecting the two different hyperfine groundstates in rubidium a phase locked loop including a frequency divider has been designed and implemented.

Light storage and retrieval has been demonstrated using a Zeeman scheme on the D_1 line. Two microsecond long classical light pulses containing one million photons on average were stored and retrieved with an efficiency of 15% after a delay of one microsecond.

Several methods of attenuating the strong co-propagating control laser beam to allow for lowering the signal pulse intensity in future experiments are discussed.

Contents

Chapter 1

Introduction

Contents

1.1 Quantum information processing

Several layouts for practical quantum information processing (QIP) networks are discussed in the scientific community [1, 2, 3]. Over the years several ideas and fundamental requirements have been distilled. The ones relevant to this thesis are the following:

1. Photons are presumably the best candidates for unperturbed long distance transfer of quantum information with possible embodiments in form of polarization, number state, time bin or rail qubits. They are also the fastest qubit carriers.
2. In a quantum network that uses photons — either as the computational qubits or for the transport of quantum information — it is desirable to buffer or delay these photons into quantum memories with a variable time delay whilst coherently preserving *all* of its quantum properties for repeating, purification, or error correction protocols.
3. Long-lived atomic states in single atoms or atomic ensembles (or more generally single emitters and emitter ensembles) are able to serve as such quantum memories but also as stationary processing nodes (quantum gates).

In linear optics quantum computation (LOQC) the only active components needed are single-photon sources and single photon detectors if all involved components were 100% efficient. The passive components are beamsplitters, phase shifters, and wave plates. In order to compensate naturally occurring inefficiencies sophisticated purification schemes using ancillary qubits and entanglement swapping have been devised that require some kind of quantum memory.

Since at least 1999 our research group has been involved with the development of a single-photon source with an intrinsic photon generation process that is inherently deterministic. At about the same time when the first atom-cavity based single photon source had been demonstrated by Kuhn et al. (2002) based on the proposals of Kimble (1997) and Kuhn (1999) good progress had been made in the field of ensemble-based slow light and light storage in the groups of Hau (1999) and Lukin (2001) specifically using the on-resonant phenomenon electromagnetically induced transparency (EIT).

For serious LOQC applications a mutually compatible pair of single-photon source and quantum memory is needed. Since both these approaches, single atom-cavity system and EIT in an atomic ensemble, use specific pure isotopes, and handle light pulses of comparable lengths it seemed fit to start investigations with the prospect of combining these two systems in hope they together could act as an elementary prototype building block for QIP.

Reliable single-photon sources are needed in many QIP schemes. Singleness in form of an antibunching signature in a second-order correlation ($g^{(2)}$) measurement has been demonstrated in a variety of system whereas the deterministic production – the "push-button" ability with close to unity success – is almost exclusively known to systems that use vacuum-stimulated Raman adiabatic passage (vSTIRAP). Also, many schemes are lacking a good collection efficiency due to emission into the entire 4π solid angle. This disadvantage is absent in systems

that use an enhanced field mode to produce and pick up the photons.

In optical cavity quantum electrodynamics (CQED) an atom is placed in between two highly reflecting mirrors. This leads to stronger interaction of the atom with the enhanced vacuum fluctuations of the allowed cavity field modes. Spontaneous emission being emission stimulated by the vacuum fluctuations of the electric field now experiences an enhancement due to the amplification from the cavity. The Purcell factor describes this enhancement. The additional emission is deposited in the mode prescribed by the enhanced vacuum field with the nice feature that it is now in a well defined spatial mode. Different mirror transmissions direct the emission to one side. The transversally applied laser field drives a stimulated Raman adiabatic passage scheme (STIRAP) together with the second branch being the vacuum field mode of the cavity. Due to the finite decay of the cavity the photon is extracted from the system. The emitted photon is evidently following the spatial mode prescribed by the cavity and thus the coupling to the following optical components is facilitated due to the knowledge of how the cavity mode continues at the out-coupling side.

In order to interconvert photonic quantum information to matter-based storage or processing units and vice versa a fully coherent control scheme is needed. This mechanism has to work on the individual quantum bit level and should allow for arbitrary time delays while maintaining a sufficiently high conversion efficiency. The storage of a single photon maximally focussed onto a single atom in free space is inefficient due to the effective cross sections being a factor of $\sim \pi^2$ off. Enhancement of the interaction can be provided by employing a cavity. The multiple reflections increase the interaction probability to one. But in order to avoid spontaneous emission one has to make use of adiabatic passaging with an additional control field so that a reversible transfer from photonic state to matter state is possible. This is sometimes called coherent "absorption". The target state for the coherent absorption is preferably a metastable

state with slow decay like a ground state.

A much easier way to increase light matter interaction is to increase the number of atoms involved in the process. In an atomic ensemble the photonic state finds enough atoms to interact with and the light is stored in a superposition of all atoms in the beam path. Plenty of research has been done where a Λ type level schemes has been used with two ground states and one excited state that couples the two involved fields. The system is assumed to be in the ground state that is addressed by the signal field. A control field on the other branch then renders the signal resonance transparent through a quantum interference of the excitation paths. This effect is accompanied by a significant change of the index of refraction and reduction of the group velocity. Controlled reduction of the control field leads to a stand still of the signal pulse and the light excitation survives as spin wave (ground state coherence). Switching the control field back on releases the signal pulse. This way the signal can be stored an arbitrary amount of time within the timescales of the fastest decay of the system. Shaping the control field during switch-off and switch-on affects the efficiency and the output pulse shape. For maximising the efficiency and achieving a target waveform the control field can be optimised. This technique is possible in all types of atomic ensembles like ultra-cold gases, Bose-Einstein condensates, hot vapours and even ensembles of artificial atoms in solids.

Both systems, the single photon source and the EIT storage, have seen much development, but as yet have not been combined to form a simple quantum network block. A sketch of such a system is shown in Fig. 1.1.

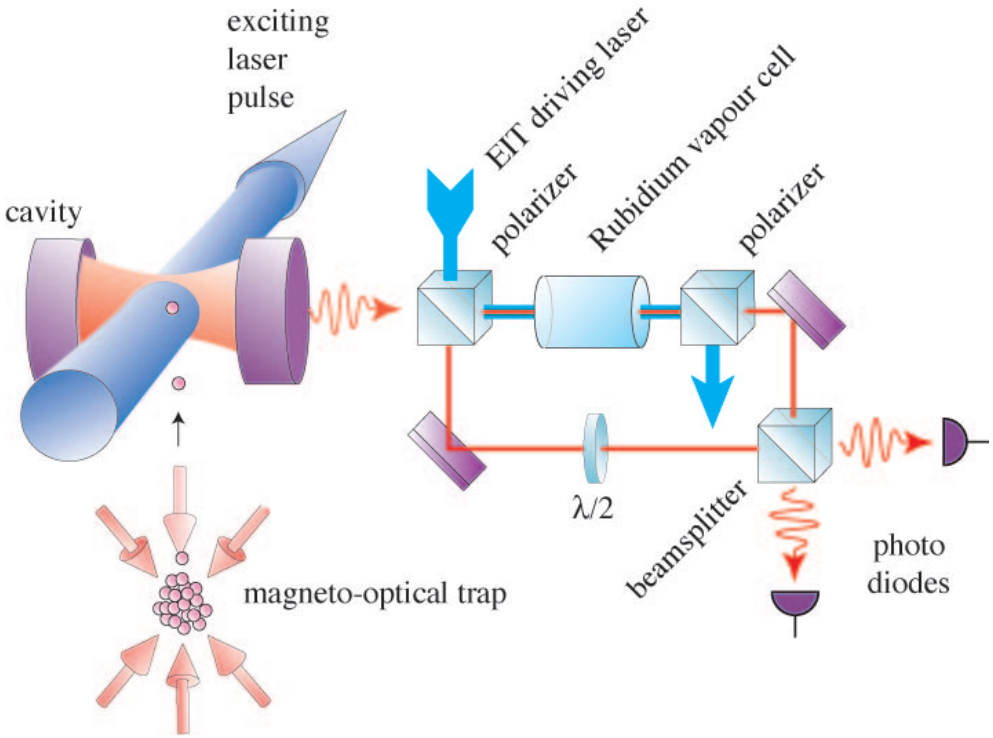

Figure 1.1 Envisioned setup to answer the original research question. Single-photons emitted from the cavity are delayed in the Rb vapour cell due to slow light effects or stored in a dark-state polariton and retrieved after an adjustable time delay. Delayed photons are then interfered on a beamsplitter with subsequently emitted photons from the cavity. The Hong-Ou-Mandel type two-photon interference will yield a measure for the quality of the photon storage process regarding the preservation of coherence. If the vapour cell is replaced with any other memory and the single photon source is well known and characterized, then this setup forms an evaluation or benchmarking kit for the memory or vice versa with a known memory for an uncharacterized photon source.

1.2 Single-photon source

Typical benchmark parameters for a high-finesse Fabry-Perot cavity with curved mirrors are the free spectral range, finesse, round trip losses, transverse mode spacing and in case of different reflectivities (optically asymmetric cavity) the output coupling. Combining two existing mirrors to a cavity leaves only the mirror spacing as a free parameter. Main requirement for the deterministic photon generation is a high production efficiency. Demanding a high production efficiency p is in most experimental cases equivalent to require the system to be in the strong coupling regime ($g > \kappa, \gamma$). Then in an adiabatically driven atom-cavity system this production efficiency cannot exceed the value $2C/(2C+1)$, where $C = g^2/(2\kappa\gamma)$ is the one-atom cooperativity. Although this formula is strictly only correct for the bad cavity regime which is defined by $\kappa \gg \frac{g^2}{\gamma} \gg \gamma$.

The practical challenge of manoeuvering one atom into the field mode of an optical cavity has been solved experimentally in different ways. With increasing technological effort and in chronological order there have been essentially three generations of single atom supply. The first was to let an cold atom cloud fall from above the cavity (Kimble). The second is to throw atoms upwards from beneath the cavity (Rempe). The third is the controlled transport with an optical dipole trap from the side (Meschede, Rempe). Also combinations of these have been applied such as falling atoms caught by an intracavity dipole trap (Kimble). It should also be mentioned that for microwave cavities hot atomic ovens are used (zeroth generation) and that trapped ions can be considered as a fourth generation of single atom supply for cavities. Again in the line of least complexity we want to exclude the additional use of a dipole trap which also adds Stark shifts that have to be taken into account and that the control of the vibrational motion in the trapping potential is doable but not trivial. Encouraging progress has been made

in this aspect using cavity cooling effects. But here we want to argue that the simplest choice is a ballistic transport from an magneto-optical trap. And we choose the fountain over the dropped cloud since the interaction time can be in the range of $\sim$1-5 ms if the turning point lies close to the mode axis as opposed to $\sim$10-50 μs when traversing at finite speed originating from a cloud well above the cavity.

1.3 Single Photon Memory

In order to process or buffer quantum information a mapping of the ephemeral photonic information onto long-term stable nodes is needed. One option is to use coherent absorption into long lived states without giving rise to spontaneous decay.

For light pulses e.g. the modified dispersion in an EIT medium leads to a reduction of the group velocity and can according to experimental conditions result in such extremely low group velocities as 17 m/s [4] which led to the term "slow light".

A medium that shows a reduction in group velocity and thus exhibits a slow light effect already acts as a delay memory. The disadvantage though is that a fixed delay requires a certain combination of control light intensity, number of atoms and length of the medium which in turn limits the spectral window and gives a minimum temporal length of the pulse. Otherwise part of the pulse is absorbed. The ratio of achievable delay (storage) time to pulse length is often used as a figure of merit for this type of system.

The interesting aspects emerge when the control field is altered in its amplitude after the signal field has been compressed, entered the medium and is inside the medium. Here, a theory has been developed that looks at the light field and the collective atomic excitations at the same time [5]. A shape preserving entity has been identified which is the sum of the light field and atomic coherence and has been named dark state polariton (DSP). The control field

hereby determines the mixing ratio of the two components with the effect that when reducing the control field intensity the DSP takes on more of the spin wave component and at the same time the photonic component reduces its velocity. This can end in the light field being completely converted to a stationary spin wave. Increasing the control field after an arbitrary time releases the spin wave. The control field, like in other adiabatic passage techniques, has to be switched smoothly so that the system follows the dark state.

In this way the delay capability of an atomic gas ensemble due to the slow light effect is extended and complemented by an additional variable time delay due to DSP mapping. This is understood as "dynamic" EIT. The interesting aspect of the DSP concept is that it does not depend on the state the probe field is in, meaning that it also applies to quantum fields and the special case of single photon states. The deliberate shaping of the EIT control field actually opened up whole new avenues of proficiently managing the output shapes of the retrieved signal field (Gorshkov, Novikova).

In a classical medium (ensemble of absorbers) the relevant magnitudes are the absorption cross section σ (units of L^2), the Number density $\varrho(L^{-3})$, and the absorption length L (L). This product is called the optical depth is dimensionless and is found in the exponent of the transmittance. The absorbance is then $1 - \exp(-\sigma\varrho L)$ accordingly. The dependence on the probe frequency comes in through the absorption coefficient or cross section.

For QIP applications a single photon wave packet should not only not be absorbed by a storage device but also not distorted. The latter happens due to the partial absorption of the wings in the spectral profile but also due to the non-linear dispersion.

For a simple experimental scheme it would be preferable if the control field without any further ado could also be used to prepare the medium by pumping the population into the ground state that serves as state 2 in the simplified Lambda level scheme. Additional laser fields that

just add to the complexity could thus be avoided. Some pumping schemes also require complex and precise timing. Another issue especially in Alkali gases relating to their level structure is to decide whether to use hf ground states or zeeman substate of one hyperfine ground level. This decision can cost several k$. As the level spacing of hyperfine ground states in alkalis cannot be bridged by shifting the laser field with medium priced components like an acousto-optic modulator (AOM), more expensive equipment like an electrooptic modulator (EOM) or an additional laser are needed. The advantage of a hyperfine scheme is that the polarization of the fields can be lin perp lin, orthogonally circular polarized or even the same circular polarization. Using hyperfine states has the additional advantage that the control field can be separated from the signal channel by a series of etalons.

A common technique to overlap the laser fields in front of the medium and to separate them after the medium is to use a polarizing beam splitter.

In fact a sufficient suppression is necessary in order to not swamp the detector with residual control laser light. But even with the hyperfine states it is important to prepare the medium in a useful way. If there are solitary levels to which population is only lost it won't facilitate the EIT scheme. In some hyperfine schemes probe and control field were produced by an EOM. Although suppression of the unused sideband was only by 90% and an adverse effect of the residual 10% has not been mentioned [6].

The full control over the output pulse shape opens up the possibility of producing time-bin qubits which also enables the control over amplitude and phase. Partial retrieval is also possible.

At very large optical depths the EIT performance can degrade due to competing nonlinear effects like four wave mixing (FWM) and due to radiation trapping. Practical light storage is thus likely be done at moderate optical depths where optimisation becomes important.

Subject to optimisation can be the signal field and the control field pulse shapes at input

and the control field at output for a desired signal shape. It's interesting to underline that if one shape is given there exists an optimum complement which stores maximally. There is no need to optimise both.

One optimisation method is the so-called time-reversal. This procedure works for given control field and given optical depth. In 2007 it has been demonstrated by Novikova et al. [7] that different initial trial pulses converge to the same optimum pulse shape and that the optimum shapes look differently depending on the control field shape but that they all had the same maximum efficiency. The spin-coherence decay during the write and retrieval stages is assumed to be low. For every optical depth there exist a unique spin wave that maximises the memory efficiency.

When reducing the control field power this increases the group index and thus reduces the group velocity, it also narrows the transparency window the question is what happens to the pulse which should still have a finite spectral width. Fleischhauer and Lukin [8] investigated this and showed that the EIT transparency window and the spectral width of the wave packet essentially (because the mixing angle is almost always close to $\pi/2$) shrink by the same factor and their ratio stays constant. For experimental purposes this means that anything can be done once the pulse has completely entered the medium which is also why one would want to have the compressed pulse much smaller than the cell to assure this and to allow for a little propagation while doing the dynamic switching. At given Rabi frequency the compression ratio can be increased by increasing the group index by increasing the optical depth.

Reflection at the medium can distort the signal field pulse shape as there is a different index of refraction in the medium with spectral dependence. An incoming pulse at normal incidence could therefore suffer partial reflection for some of its spectral components.

If beams are almost co-propagating but with a small angle between them the spin wave picks

up a spatial phase according to $\Delta k = k(1 - \cos\vartheta)$. The polariton is then sensitive to variations in the atomic positions. Atomic motion would lead to a dephasing. To retain a high fidelity the atomic motion would have to be restricted to much less than $\lambda/(1 - \cos\vartheta)$.

If the ground states are degenerate then backward retrieval is more efficient than forward retrieval. If their energy splitting is finite forward retrieval is more efficient [9, 10, 11].

In order to store a photon every part of the wave packet should be reliably stored and retrieved. If the medium is only to be used as a linear slow light delay it does not matter if the pulse fits into the medium. Distortion occurs only due to the spectral wings being absorbed by the medium. The slower the group velocity the more the pulse gets distorted.

It should be noted that a single photon storage does not equal a qubit storage but rather that in the case of polarization qubits two rails of identical storage schemes have to be implemented. time bin qubits would be possible though.

Many schemes are known for light field storage in atomic ensembles, some are also applicable in solids. Amongst these are EIT, Raman, Photon echo, CRIB. Extensive experimental and theoretical research has been done on Optimal Storage (Gorshkov, Novikova).

In a compendium of publications Gorshkov et al have extensively studied the Photon storage. They identified the resonant optical density of an ensemble as the only important figure of merit for storage and retrieval processes (EIT as well as Raman and photon echo schemes were considered). In the limit of infinitely large optical depth and negligible decoherence between the ground states, the scheme is 100% efficient in storing and retrieving any input signal field. Also from the spin wave a specifically shaped control field can shape the output pulse shape into any arbitrary form. For real ensembles with a finite optical depth efficiency is bound to a value below unity. At finite optical depth the memory efficiency becomes dependent on all involved pulse shapes, i.e. not only has the control field an optimal shape with respect to an arbitrary

input field but also vice versa.

During retrieval there is fixed branching ratio between contructive forward interference (desired light) and undesired polarization decay rate. Major assumption that were made in that work that control and signal field are narrowband fields. Also reabsorption of sponatneously emitted photons (light trapping/depumping) was negelcted. The biggest concern with spoantaneously emitted photons is if they are emitted into the retrieval mode. This happens with a probability proprtional to the far field solid angle $\sim \lambda^2/A \sim d/N$, with A the cross section of the beams and d the on-resonant optical depth. They also proved that the fraction of incoming photons lost due to spontaneous emission decreases with increasing optical depth. Care has to be taken with the inital preparation. Another assumption that is made, that the control beam is much wider tha nthe signal beam so that the transverse profile of the control field can be considered constant.

1.4 A Practical System

Although first experiments in optical CQED were done with caesium and first experiments in EIT have been done with a variety of different elements, rubidium is today the workhorse most research groups rely on in both fields. This is owed to the fact that the frequencies of inexpensive diode lasers needed for the D_1 and D_2 lines in rubidium coincide with the compact disc industry standard. Rubidium also has a sufficient vapour pressure at room or higher temperatures.

While theoretical models are usually based on three-level schemes, in practise it might not be straightforward to identify a suitable level scheme, or conversely additional effects based on the influence of a multi-level structure need to be taken into account.

A good Λ system should be easy to prepare, provide a high light storage efficiency and be able to be made resilient to dephasing effects.

High-finesse cavities provide a stronger atom-photon interaction and enable the controlled processing of the incurred wave packets. The conversion of photonic quantum information to stationary nodes such as atoms is a vital requirement for gate operations with less auxiliary photonic qubits. In order to invert the emission process of a single photon, i.e. to "absorb" a photon in a controlled way a reversible Hamiltonian evolution between two long-lived states is needed which is missing in most deterministic single-photon sources [12, 13, 14, 15, 16, 17, 18, 19] where an electronic excitation decays spontaneously precluding its reversal. The STIRAP technique used in atom-cavity systems is intrinsically reversible and hence allows for unitary operation [20]. Photons in free space do not decohere and are thus robust carriers of QI. Practical transmission of single photon states is done in glass fibre transmission lines. The inevitable absorption losses require some sort of repeater structure. With single photons this demands for memories and error correction codes.

Strictly speaking photonics qubits (flying qubits) cannot really be buffered or delayed by other means than increasing the optical path length. A different approach is to convert the flying qubit into a stationary qubit usually by converting it into an equivalent superposition of electronic states in matter (although there are also newer concepts using states of the nuclear spin). Two different approaches exist: using a single emitter, e.g. an atom, ion, or quantum dot, or using an ensemble of single emitters. Since conversion onto the former is usually limited to efficiencies well below unity the latter can at least in theory provide 100% conversion efficiency.

In our setup we use a vapour cell with buffer gas as storage medium and use electromagnetically induced transparency (EIT) as mechanism to store the photonic information. One important thing has to be kept in mind: The photons emitted from the cavity are several hundred meters long in free space and therefore they need to be compressed to fit into the medium. EIT with its special dispersive property provides the ability of such compression of temporal

pulse envelopes.

Since the control laser creates a transparency in midst of an absorption line and since absorption and refractive index are deeply connected via the Kramers-Kronig relations the transparency peak inadvertently leads to a corresponding feature in the dispersion and with the right choice of the control field strength to a region of highly linear and steep normal dispersion where there is usually anomalous dispersion. The slope of the refractive index in this region leads to a very high group index and thus to very low group velocity. I.e. pulses experience a tremendous slow down. Since EIT also provides transparency in this region light pulses can pass the medium at speeds much lower than the vacuum speed of light while not be significantly attenuated.

Although the above description assumes a constant control field first experimental observations have been made with pulsed control fields. Some of today's research interests in EIT are motivated by its potential use for quantum memories, and even its application as a phase gate.

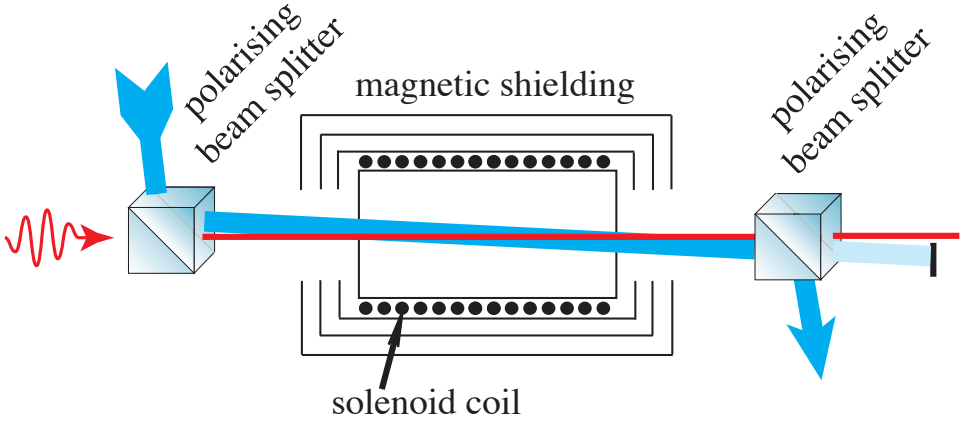

Figure 1.2 A potential configuration for light storage: single photons, or a weak probe beam (red), would be incident on a vapour cell (surrounded by the heating solenoid coil and magnetic shielding), in the presence of an orthogonally polarized coupling field (blue). This figure demonstrates two filtering techniques: polarization-selection, and angular deviation.

A quantum memory which can coherently store and retrieve a single photon is an important tool for long distance quantum communication and quantum computing [21]. Quantum communication such as cryptographic key distribution over optical fibres is already practical over

tens of kilometres [22], but could be extended using quantum repeaters [23, 24], which features a quantum memory.

To that end, this project is a preliminary investigation into a realisation of quantum memory with EIT. Naturally, there are other possible approaches (see [21]) but EIT has shown promise: weak pulse storage has been achieved with this approach in hot ^{87}Rb [25] vapour, ultracold Na [26] and solid state systems [27]. Moreover, storage of single photons has been demonstrated in ultracold ^{85}Rb [28] and hot ^{87}Rb vapour [29].

Chapter 2

Theory

Contents

This chapter starts with a discussion on the requirements for an EIT-based quantum memory. The following sections review EIT in three-level systems at rest without any further interactions and then gradually realistic parameters are added and their influences are discussed.

2.1 Memory requirements

An ideal quantum memory should simply be some "black box" that can store a quantum state and later be able to return this state without loss or distortion. These quantum states do not necessarily need to be quantum *bits*. It could be a superposition state of any number of states and with any arbitrary coefficients. But certainly a memory for a qubit would seem the simplest of quantum memories. Also, if there is a way of splitting the quantum state into the weighted contributions of its basis states (logical states) and store them separately and recombine them upon readout this would simplify things.

In Linear Optics Quantum Computation (LOQC) quantum information (i.e. a state superposition) is imprinted on some electromagnetic field in form of polarisation or time bins. With

both of these separating the logical states is easy and thus the problem narrows down to providing a single photon memory which in itself might not be easy. But even if this can be achieved with a high readout fidelity and high readout efficiency that still does not necessarily mean that two qubit memories of that same kind will maintain entanglement.

2.2 Theoretical background

2.2.1 Linear optical response

EIT [30] is a phenomenon in which one electromagnetic field (the coupling or control) can render a medium transparent to a second field (the probe or signal). The basic theory of EIT and associated effects is covered in [31, 32, 33] and I follow their analysis here. We start with two classical $\vec{E}$ fields interacting with a subset of three atomic energy levels in a Λ-system shown in Fig. 2.1.

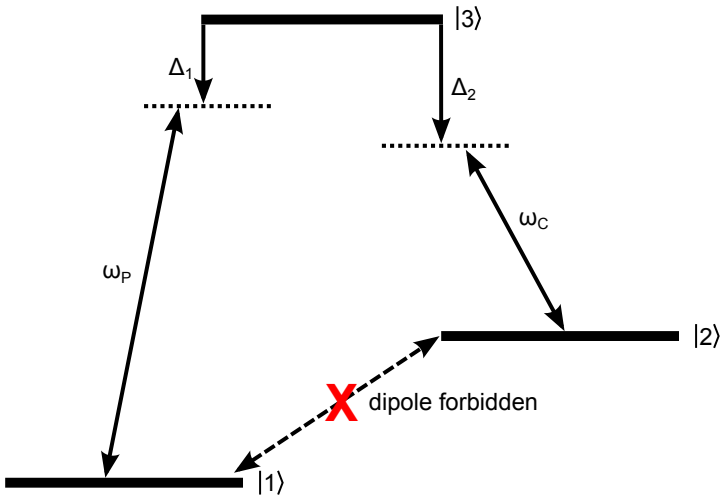

Figure 2.1 A three level Λ-scheme featuring a probe beam with frequency ω_{p} detuned from ω_{31} by Δ_1 and a control beam of frequency ω_{c} detuned from ω_{32} by Δ_2. The transition $|2\rangle \rightarrow |1\rangle$ is dipole forbidden.

Since we observe EIT phenomena in macroscopic media, it is essential to explicitly consider each atom as a subsystem of the medium. Thus the evolution of each atom must be described

using density operators. The evolution of these operators consists of a coherent and incoherent part which are assumed to vary independently [34, p.356]:

$$\dot{\rho} = \frac{1}{i\hbar}[H_{\mathrm{A}} + H_{\mathrm{int}}, \rho] + (\dot{\rho})_{\mathrm{inc}} \quad , \tag{2.1}$$

where H_{A} is the atomic Hamiltonian and H_{int} the interaction Hamiltonian between the atom and the $\vec{E}$ fields, given by

$$H_{\mathrm{int}} = -\vec{d} \cdot [\vec{\mathcal{E}}_{\mathrm{p}} \cos\omega_{\mathrm{p}} t + \vec{\mathcal{E}}_{\mathrm{c}} \cos\omega_{\mathrm{c}} t] \quad , \tag{2.2}$$

where $\vec{d}$ is the dipole operator. The incoherent evolution $(\dot{\rho})_{\mathrm{inc}}$ takes into account the effects on the populations and coherences of ρ from the spontaneous decay of $|3\rangle$ to $|2\rangle$ (Γ_{32}) and $|1\rangle$ (Γ_{31}) given by the master equation (2.1) [34]. We also include three decay constants γ_3, γ_2 and γ_1 which phenomenologically quantify the decay by other means of coherences involving the states $|3\rangle$, $|2\rangle$ and $|1\rangle$ respectively. Writing the total spontaneous decay rate as $\Gamma_3 = \Gamma_{32} + \Gamma_{31}$ and the total decay rates of the coherences as $\gamma_{21} = \gamma_2 + \gamma_1$, $\gamma_{31} = \Gamma_3 + \gamma_3 + \gamma_1$ and $\gamma_{32} = \Gamma_3 + \gamma_2 + \gamma_3$ the incoherent evolution in the basis $\{|1\rangle, |2\rangle, |3\rangle\}$ can be written [31] as:

$$(\dot{\rho})_{\mathrm{inc}} = \frac{1}{2} \begin{pmatrix} 2\Gamma_{31}\rho_{33} & -\gamma_{21}\rho_{12} & -\gamma_{31}\rho_{13} \\ -\gamma_{21}\rho_{21} & 2\Gamma_{32}\rho_{33} & -\gamma_{32}\rho_{23} \\ -\gamma_{31}\rho_{31} & -\gamma_{32}\rho_{23} & -2\Gamma_{3}\rho_{33} \end{pmatrix} \quad . \tag{2.3}$$

Applying the rotating wave approximation [35], H_{int} can also be written in the interaction

picture in this basis as:

$$H_{\text{int}} = -\frac{\hbar}{2}\begin{pmatrix} 0 & 0 & \Omega_{\text{p}}e^{-i\Delta_1 t} \\ 0 & 0 & \Omega_{\text{c}}e^{-i\Delta_2 t} \\ \Omega_{\text{p}}e^{i\Delta_1 t} & \Omega_{\text{c}}e^{i\Delta_2 t} & 0 \end{pmatrix} \quad , \tag{2.4}$$

where the Rabi frequencies are given by e.g. $\hbar\Omega_{\text{p}} = \langle 1|\vec{d}|3\rangle \cdot \vec{\mathcal{E}}_{\text{p}}$. The elements of the density matrix can be related to the polarisation[1] of a medium with an atomic density ϱ by:

$$\begin{aligned} \vec{P} &= \varrho\langle\vec{d}\rangle \\ &= \varrho\text{Tr}(\rho\vec{d}) \\ &= \varrho[\vec{d}_{13}\rho_{31}e^{i\omega_{31}t} + \vec{d}_{23}\rho_{32}e^{i\omega_{31}t} + c.c.] \quad . \end{aligned} \tag{2.5}$$

Finally the polarisation and complex linear susceptibility are related [32] according to:

$$\vec{P} = \tfrac{1}{2}\varepsilon_0\vec{\mathcal{E}}_{\text{p}}[\chi e^{-i\omega_{\text{p}}t} + \chi^* e^{i\omega_{\text{p}}t}] \quad , \tag{2.6}$$

so that the complex susceptibility is given by:

$$\chi(\omega_{\text{p}}) = -\frac{2\varrho|d_{31}|^2}{\varepsilon_0\hbar\Omega_{\text{p}}}e^{-i\Delta_1 t}\rho_{13} \quad . \tag{2.7}$$

We now just solve (2.1) for the steady state, assuming that $\Omega_{\text{p}} \ll \Omega_{\text{c}}$ ($\rho_{11} \simeq 1$) to find ρ_{13}. The result is substituted into (2.7), and written [31] in terms of the one-photon detuning $\Delta = \Delta_1$

[1] the exponentials arise in the conversion of ρ to the interaction picture

and two-photon detuning $\delta = \Delta_1 - \Delta_2$:

$$\chi(\omega_{\rm p}) = \frac{2\varrho|d_{31}|^2}{\varepsilon_0\hbar}\left[\frac{2\delta(|\Omega_{\rm c}|^2 - 4\delta\Delta) - 2\Delta\gamma_{21}^2}{||\Omega_{\rm c}|^2 + (\gamma_{31} + i2\Delta)(\gamma_{21} + i2\delta)|^2}\right.$$
$$\left. + \mathrm{i}\frac{4\delta^2\gamma_{31} + \gamma_{21}(|\Omega_{\rm c}|^2 + \gamma_{21}\gamma_{31})}{||\Omega_{\rm c}|^2 + (\gamma_{31} + i2\Delta)(\gamma_{21} + i2\delta)|^2}\right] \quad . \tag{2.8}$$

Now moving to an optically thick medium[2], the initial and final probe fields are related by the transfer function $T = \exp[ik_{\rm p}z\chi/2]$ so that:

$$\begin{aligned}\vec{E}_{\rm f} &= T\vec{E}_{\rm i} \\ &= \vec{\mathcal{E}}e^{-k_{\rm p}z{\rm Im}[\chi]/2}e^{i((k_{\rm p}+{\rm Re}[\chi]/2)z-\omega_{\rm p}t)} \quad .\end{aligned} \tag{2.9}$$

We see that the real part of χ gives a contribution to the wavenumber, i.e. changes the speed of the wave, and the imaginary part gives an exponentially decaying pre-factor, attenuating the wave.

Consider the form of Im[χ], plotted in Fig. 2.2 for the idealised case of zero ground state decoherence γ_{21}. With no control field the probe has a normal absorption profile centred on the $\omega_{\rm p} = \omega_{31}$, but when a control field is applied at a detuning of $\Delta_2 = 0.2\gamma_{31}$, the absorption drops to zero in an asymmetric dip centred on the two-photon resonance[3] $\delta = 0$. This tells us that in the idealised system at least, an opaque medium can be made transparent, regardless what the control power is or the decoherence γ_{31}.

[2]In doing so, it is customary to adjust the normalising pre-factor of χ to be in terms of the coupling constant to the probe field, $\eta = (3/4\pi^2)c\varrho\Gamma_{31}\lambda^3$, where $\eta k = \varrho\sigma$, σ is the absorption cross section, and λ is the wavelength of the $1 \rightarrow 3$ transition.

[3]In fact, the true minimum of the absorption is not quite at the two photon resonance, for typical cases of EIT it is at [36] $\Delta_1 = (1 - \frac{\omega_{21}}{\omega_{32}})\Delta_2$.

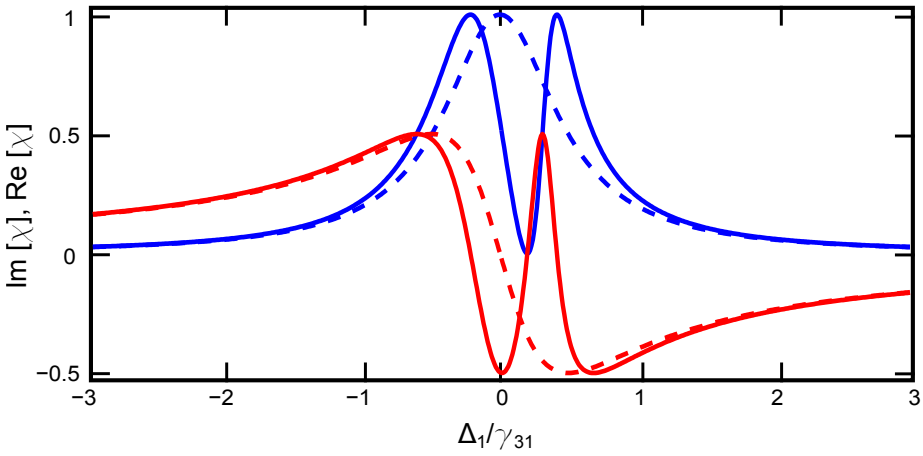

Figure 2.2 Real part (in red) and imaginary part (in blue) of the susceptibility in units of $\frac{2\varrho|d_{31}|^2}{\varepsilon_0\hbar}$ as a function of the probe detuning normalised to the excited state decay rate Δ_1/γ_{31} for stationary atoms. The FWHM is for the dashed absorption profile is therefore 1. Control detuning is $\Delta_2 = 0.2\gamma_{31}$ and γ_{21}=0. Solid lines are for $\Omega_c = 0.2\gamma_{31}$ and dashed lines are for $\Omega_c = 0$.

Suppose that $\gamma_{21} \neq 0$. Then for $\Delta_1 = \Delta_2 = 0$ the pre-factor is given by:

$$\exp[-k_p z \mathrm{Im}[\chi]/2] = \exp\left[-\varrho\sigma z/\left(\frac{|\Omega_c|^2}{\gamma_{21}} + \gamma_{31}\right)\right] \quad . \tag{2.10}$$

So although the medium is no longer 100% transparent for all control powers, by increasing the control power sufficiently we can recover this transparency. It also shows how important it is to limit the ground state decoherence. For experiments with hot gases such as ours, decoherence can be caused by dephasing collisions between rubidium atoms or between atoms and the walls of the cell. They can also be caused by stray magnetic fields switching atoms between the ground states. Finally, for atoms addressed with laser beams of finite diameter, the high average speed ($\sim$300 m/s) of the atoms and low density means they move through the beam path very quickly, exchanging the atoms in the beam with those outside. A buffer gas removes the probability of Rb-Rb collisions and reduces the mean free path localising the atoms in the beam path. Also, magnetic shielding with μ-metal can reduce the effects of stray magnetic fields.

To see what type of feature we expect, we can expand (2.9) around the absorption minimum. The lineshape in this special case ($\Delta = 0$) is a Gaussian with a full width at half maximum given by:

$$\text{FWHM} = \frac{(|\Omega_c|^2 + \gamma_{31}\gamma_{21})}{\sqrt{\Gamma_{31}\gamma_{31}\varrho\sigma z}} \quad . \tag{2.11}$$

This suggests a quadratic dependence between the FWHM of the EIT feature and the Rabi frequency, and also a narrowing of the transparency window as the medium length or atomic density increases.

Our experiment is conducted with a Rb atomic vapour at between 50°C and 80°C to increase the atomic density. The moving atoms 'see' a Doppler shifting of the incident light. In a configuration where both fields are co-propagating, the shift is the same for both the probe and the control, so the point at which the two-photon detuning occurs remains the same as the probe frequency is varied. For the idealised three level system with a large spacing between the low lying levels, the EIT window is left unchanged, but the underlying absorption peak is Doppler broadened in the usual way. A typical value for such a width at 75°C is 560 MHz.

The situation is more complex for systems where either the separation between $|2\rangle$ and $|1\rangle$ or between $|3\rangle$ and other neighbouring levels in the excited state is less than the width of the Doppler broadened absorption peak. The result in the first case is that the Doppler broadening can 'wash out' the level separation [31]. In the second case atoms will absorb control light when their frequencies are shifted onto the nearby resonances, and decay into $|1\rangle$. Because the control is much stronger than the probe one result is pumping from $|2\rangle$ to $|1\rangle$, but we also see a variety of non-trivial velocity selective pumping effects[4] [37]. To evaluate these situations properly, it is necessary to weight the susceptibility with a distribution of frequencies derived from the Maxwell velocity distribution along the beam propagation axis, then integrate over all

[4] see the side absorption dips on Fig. 5.3

frequencies. It may also be necessary to consider other energy levels in theoretical calculations. When these calculations are performed, it is found that inhomogeneous broadening in these more complex level schemes reduces the overall height of the EIT transparency peak [38], to the detriment of a quantum memory.

2.2.2 Slow light and storage

As we saw from (2.9), the real part of χ is responsible for a dramatic slowdown in the group velocity of light. Speeds of 17 m/s have been observed [39] in BECs and 8 m/s in hot Rb [40]. The effective wavenumber for light in an EIT medium is given by (2.9) as $k_{\text{eff}} = k + \frac{1}{2}\text{Re}[\chi]$, where k is the wavenumber in free space, $\omega = ck$. The expansion of k_{eff} around $\delta = 0$ for fixed Δ_2 to second order in ω_p is:

$$k_{\text{eff}} = \left[k + \tfrac{1}{2}\text{Re}[\chi]\right]_{\delta=0} + \left[\tfrac{1}{c} + \tfrac{1}{2}\tfrac{d\text{Re}[\chi]}{d\omega_{\text{p}}}\right]\delta_{\delta=0} + \left[\tfrac{1}{4}\tfrac{d^2\text{Re}[\chi]}{d\omega_{\text{p}}^2}\right]\delta^2_{\delta=0} \quad . \tag{2.12}$$

The first term is just a constant phase shift, the factor in front of δ is the inverse of the group velocity and the factor in front of δ^2 is the group delay dispersion (GDD) per unit length in the medium [41]. From [31] we find that $\text{Re}[\chi] = \frac{2c\varrho\sigma\Gamma_{31}\delta}{|\Omega_{\text{c}}|^2+\omega_{31}\omega_{21}} + \mathcal{O}(\delta^2)$, so:

$$v_{\text{g}} \simeq c\left[1 - \frac{c\varrho\sigma\Gamma_{31}}{|\Omega_{\text{c}}|^2 + \omega_{31}\omega_{21}}\right] \quad . \tag{2.13}$$

Observing slow light is most easily done by comparing the arrival times of a reference pulse and a pulse passing through the medium. However, an important difference between (near) monochromatic continuous wave (cw) propagation and pulse propagation is that short pulses intrinsically consist of multiple frequency components, where the temporal length and spectral

width are inversely related. Thus the width of the EIT window puts a lower limit on the pulse length which can be transmitted without loss, since the spectral width of the pulse must be smaller than the EIT width [42]. There is an inherent conflict between (2.13), (2.11) and (2.10) in achieving pulse slowdown; the lower the Rabi frequency the slower the group velocity, but this gives a smaller spectral width and height of the EIT feature, leading to more absorption. Indeed, v_g cannot be reduced to zero for static control fields. However, if the control beam is adiabatically reduced to zero while the pulse is in the medium, the group velocity can be reduced to zero and the pulse will be stored as a coherence between $|1\rangle$ and $|2\rangle$. Since the leading edge of the probe pulse is slowed down before the trailing edge enters the medium, the pulse will be compressed. By choosing suitable parameters, it is possible [25] to compress the pulse to such an extent that it will fit entirely within the medium. Also, the second order terms in Re[χ] can be made to go to zero if $\Delta_1 = 0$, so in this case the GDD will be zero. The pulse can later be retrieved by switching the control beam back on [43]. See [44, 11, 45] for a full theoretical treatment.

2.3 Absorption model and fit routine

In order to gain understanding of a thermal Rb ensemble and to be able to predict absorptive behaviour, optical depth, Doppler broadening, pressure broadening and pressure shift it is useful to have a model at hand that describes Rb including the influence of a buffer gas. An outstanding publication in this field is the work of Siddons *et al.* [46] that carefully develops the full spectrum of the D lines in rubidium. The authors were so kind to provide a Mathematica script called "absdisD1.nb" on their web page. Studying this script and the following transcription into Matlab brought a big leap in understanding how to calculate a Doppler broadened spectrum. In the code one can find the following comment: *"This notebook will take ∼8 min to*

run." Although the script is from Dec. 2007 and I discovered it for the first time in late 2011 processing power of computers had not improved enough to significantly reduce the execution time. The script still needed about 5 min to finish.

After playing around with it for a while I decided to implement my own version in MatLab which could be suspected to run faster when the frequency axis (free variable) did not contain too many points. It turned out that even for 10,000 data points the script essentially finishes immediately (less than one second). Building on this it was a simple task to phenomenologically include pressure broadening and pressure shift by adding the respective values to the natural line width and the frequency offset of the resonances. Altering the isotopic fractions was also very easy.

This altered model was used to provide spectral fits to spectra at different temperatures and for different vapour cells and different isotopic composition.

And because the execution time was so much faster than in the Mathematica implementation I was able to use it as a fit routine. An example for one of these fits can be found in Ch. 4.

Implementing the fit routine held a couple of surprises. For example could the temperature be measured this way. But when observing that some of the fits for the 99.9% ^{87}Rb cells had a considerable deviation in some section of the spectrum I started letting the script find an optimal value for the isotopic fraction and it turned out that the 99.9% were actually just 98.2% (for results that confirm this assertion see section 4.2.2). Therefore a spectrum is really just like a fingerprint and many parameters can be determined at once.

Chapter 3

Experimental Setup

Contents

As some parts of the experimental setup have already been mentioned in the discussion in the theory chapter, this chapter provides a detailed description of the experimental components, setups and experimentation schemes. First the equipment used is introduced such as lasers, beam preparation, magnetic shielding, vapour cells, photodetectors, signal sources, and data acquisition. Then the different experimental setups for characterisation of the components and for the measurements are described.

3.1 Equipment

3.1.1 Rubidium vapour cells

The vapour cell used to initially investigate the EIT phenomenon was a 75 mm long spectroscopy cell filled with a natural abundance of rubidium isotopes. The atomic density of ^{87}Rb

in such a cell in atoms/m^3 is [47]

$$\varrho = \frac{37.1}{k_{\mathrm{B}}T} 10^{(7.668 - 4215\mathrm{K}/T)} \quad . \tag{3.1}$$

The temperature T was controlled by two heating coils, and could reach 85°C. A copper wire was wound in a twisted pair configuration to avoid permanently applying a magnetic field to the cell. The cell was surrounded by a μ-metal shield to block stray magnetic fields, and by a solenoid (length 310 mm, 140 turns) which could be used to de-magnetise the μ-metal shield by briefly applying an alternating current. When the investigations turned to the D_1 line, this solenoid was also used for applying a magnetic field to the cell if required. This meant there was no magnetic shielding of the cell during some of the spectroscopy results, which lead to increased decoherence. The slow light and storage results were taken without this magnetic field, so the μ-metal shield could be used as intended.

In order to successfully store light, the atoms that are in the dark-state superposition must stay in the beam path long enough such that they can be read out again after a set delay of time. At room temperature (50°C), the peak of the Boltzmann velocity distribution for rubidium atoms is at $\sim$300 ms^{-1}. Without buffer gas the mean free path is on the order of metres which means there is only ballistic flight through the beam path and the flight time through the beam is on the order of μs. By adding a buffer gas to the cell, the rubidium atoms suffer collisions and move in a diffusive fashion rather than ballistically. This helps localise the atoms. In order to not destroy the ground state coherence the depolarisation cross section should be much larger than the collisional cross section. This is the case for the noble gases. An unwanted effect of the collisions with the buffer gas atoms (or molecules) is additional broadening. This collisional broadening affects the Lorentzian natural line width and a broadening coefficient is simply added to the natural line width. Therefore, the choice of buffer gas can be vital. Similar to

many other experiments, neon was chosen as a buffer gas in the ^{87}Rb cells because it causes the smallest additional broadening [48].

Rotondaro et al. [48] provide a detailed overview for several buffer gases (noble gases and molecular gases) and their effect on the Rb D lines. Of the noble gases neon has the smallest pressure broadening coefficient (D_1 line: 0.90±0.02 MHz/Torr [48]).

3.1.2 Magnetic Shielding

A triple magnetic shield was ordered from Magnetic Shield Corp. The shield consists of three cylinders arranged like a Russian doll (see Fig. 3.1), is made from μ-metal and has a wall thickness of 0.64 mm. The diameters of the cylinders are 21, 18, and 15 cm. Their lengths are 42, 40, 38 cm. In addition, a roll of thin μ-metal foil was available which could be cut with a pair of scissors. This foil was mainly used for shielding standard cells from the magnetic field of the Faraday isolators in the laser setup. I also fabricated a cell and shield mount in the workshop (Fig. 3.2) that supported the magnetic shield on two copper tubes in order to provide a cold spot on the side of the cell.

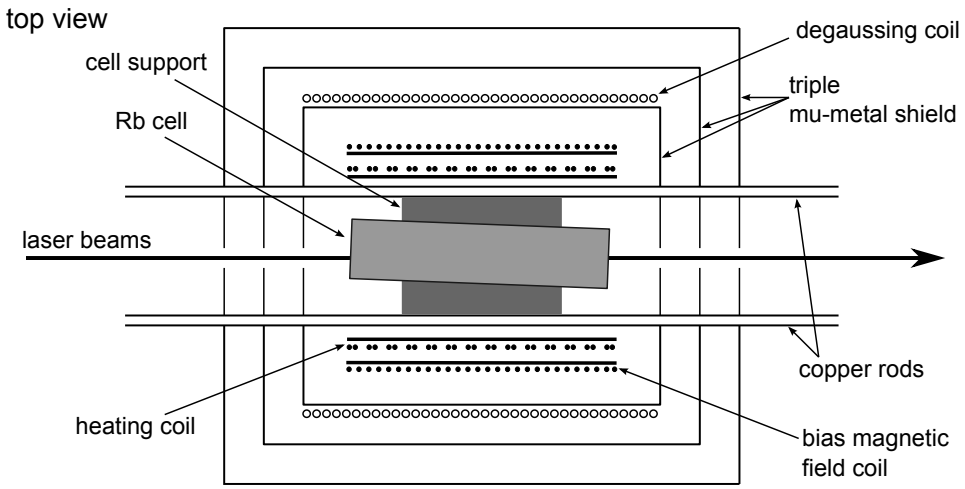

Figure 3.1 Sketch of the experimental vapour cell suspended in a triple magnetic shield.

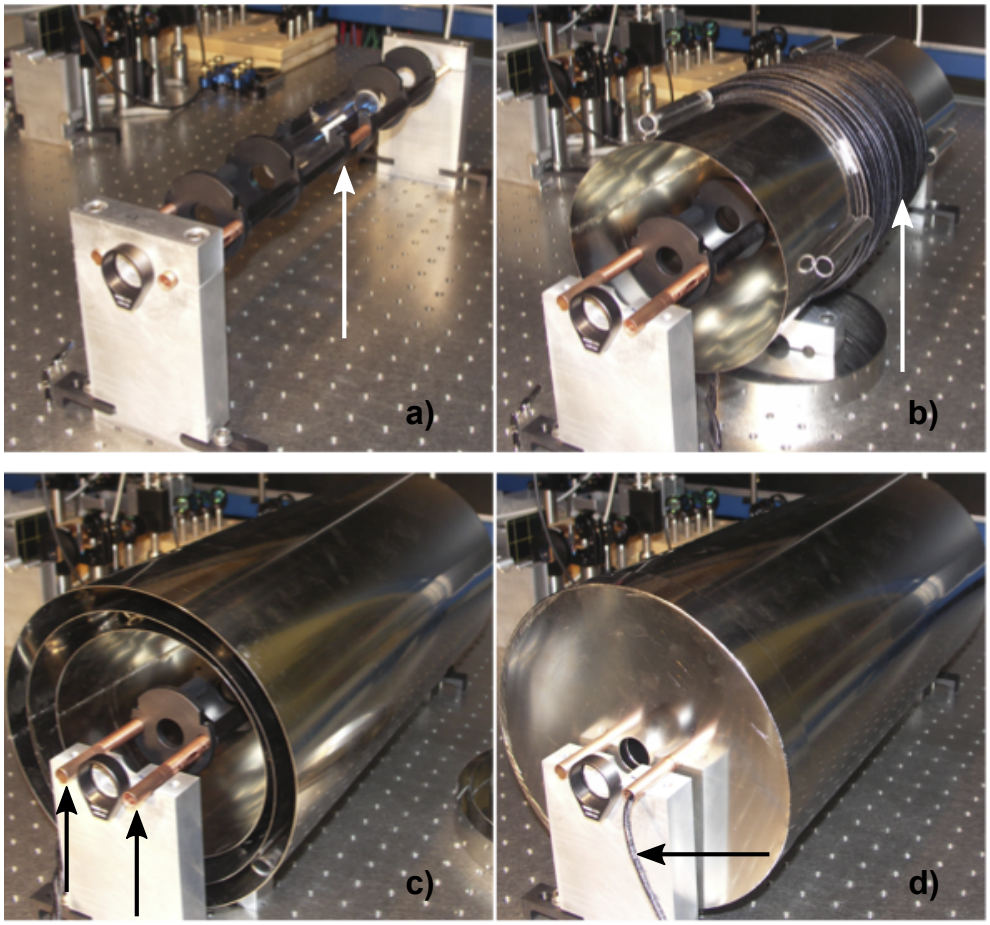

Figure 3.2 The self-made cell and magnetic shield mount. a) A u-shaped trough holds the experimental Rb vapour cell and is suspended on two copper pipes. The spacers support another tube carrying a solenoid coil to produce bias magnetic fields. b) The innermost shield has about 100 turns of wire for the purpose of degaussing. c) The magnetic shield was ordered with additional holes next to the center holes. All three cylinders rest on the copper tubes. d) One of the copper tubes would also serve as a wire feedthrough for the heating and magnetic coils inside the shielding. When using this shield a computer fan would create a small air current that is passed through a PVC hose to the other copper pipe. This way the copper pipe would take heat away from the cell mount and create a cold spot.

In the end the whole mounting system was so complex that changing the cell would take several hours. Because the simple μ-metal foil provided enough shielding when wrapped in several layers this simpler shielding was used for most of the measurements.

In other groups' work the heating is achieved with hot water running through a silicon hose that is wound around the cell. [49]

3.1.3 Fabry Perot

The group's standard design for a confocal Fabry-Perot resonator consists of two curved mirrors with radii of curvature R_c=100 mm and spacing d=100 mm. The spacer is a tube made from invar. One of the mirrors is glued directly onto one of the tube ends, the other is glued onto a piezo tube or ring which in turn is glued onto the other side of the invar spacer. This allows for spectral scanning by applying a voltage to the piezo. This functionality was used to check if the ECDLs were running single mode. Without the piezo scanning the Fabry Perot could be used as a frequency marker which was used in the vapour cell characterisation. The free spectral range is 750 MHz. The line width was measured to be approximately $\sim$1 MHz, the finesse is therefore $\sim$750 which matches the calculated finesse of 625 knowing the specified reflectivity values of the mirror coatings of R=0.995.

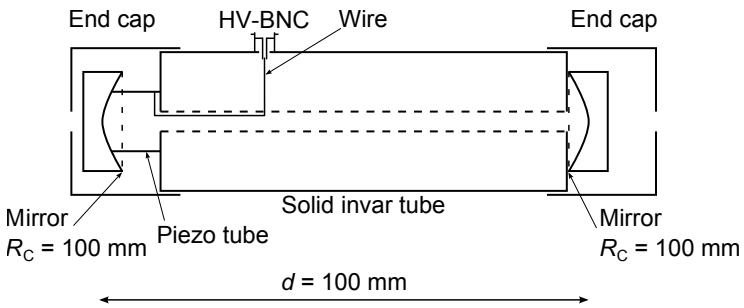

Figure 3.3 Sketch of the group's confocal Fabry-Perot design. It is frequently used to check that a laser is running single-mode by monitoring a small portion of the laser.

3.1.4 Acousto-optic modulators

To alter the intensity and frequency of the laser beams acousto-optic modulators (AOMs) from Crystal Technology, Inc. models 3080-120 and 3110-120 were employed. The AOMs in use consisted of a piezoelectric material attached to one end of a TeO_2 crystal. When an RF frequency Ω is applied to the piezo, the rapid contractions and expansions form a travelling longitudinal wave in the crystal, with alternating denser and more rarefied regions causing a varying refractive index of wavelength $\Lambda = 2\pi v_s/\Omega$ [50]. This acts as a diffraction grating moving at the speed of sound, and light scatters off the wavefronts, interfering constructively in the manner of Bragg diffraction. The scattered beam travels at an angle θ to the normal, where $\sin\theta = n\lambda/2\Lambda$, and λ is the wavelength of light [51]. Momentum conservation implies that a photon scattered into the 1st order has its frequency increased by Ω, and one scattered into the -1st order has its frequency decreased by Ω [50], so the frequency of the photon can be increased or decreased by the driving frequency. Moreover, by modulating the amplitude of the RF wave applied to the piezo, the fraction of the beam which is deflected can be modulated.

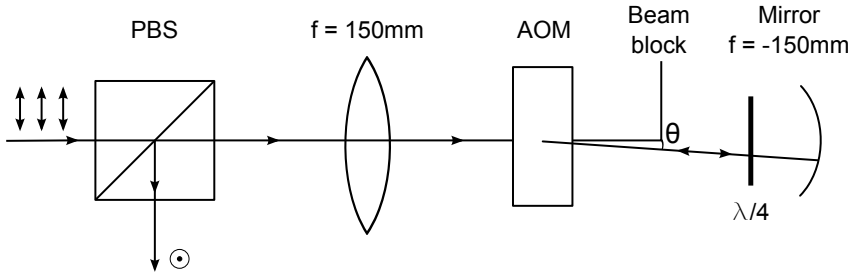

Figure 3.4 Double-pass AOM setup.

The AOM setup used can be seen in Fig. 3.4. The light was focused by a lens to ensure that the beam was well within the small TeO_2 crystal. The desired diffracted order (-1st is shown) passed through an iris while the others were blocked. To avoid Ω dependent beam deviation predicted in the previous equation, the diffracted order was reflected back along the same beam

path with a concave mirror, which also refocused the beam. Double-passing the AOM in this way also doubles the frequency change to twice the driving frequency. The reflected beam was reflected to lie in the original beam path, and unwanted orders were again blocked. To separate the incoming and outgoing beams, the input beam was linearly polarised along one axis, then a quarter wave plate in front of the concave mirror was used to rotate the reflected beam's polarisation by 90°. A polarising beam splitter could thus remove them as shown.

The AOMs could be controlled with custom driver boxes, or with an arbitrary waveform generator (LeCroy ArbStudio) controlled from the experimental computer. The latter was preferable as it allowed custom modulation patterns to be applied to the beams at a sample rate of 1 GS/s, and it also provided more stable driving frequencies.

To scan across the EIT feature when both beams are taken from the same laser, the laser was locked using a reference cell and the frequency of the probe laser beam was modulated using one AOM, keeping the control frequency fixed with another. However, the intensity of the double-passed beam is dependent on the driving frequency. For the AOMs here the driving frequency with the best efficiency was measured at 70 ± 1 MHz, and the bandwidth (FWHM) around this peak was 40 ± 4 MHz. The variation of intensity with frequency could distort the frequency scans of the EIT feature; to correct for this a PID feedback loop using the reference photodiode was implemented. This keeps the light intensity at a fixed level.

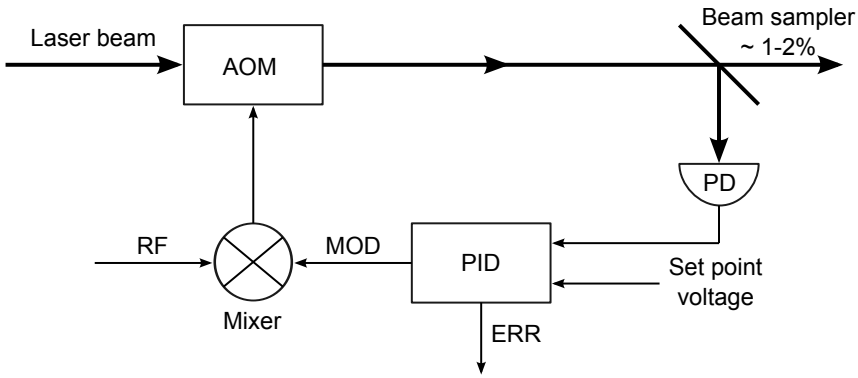

Figure 3.5 Setup for stabilising the power of a laser beam when the laser was scanned in frequency. A beam sampler deflects a few percent of the beam power onto a photodiode (PD). At the input of a PID regulator the photodiode signal is subtracted from a constant set voltage to give an error signal (ERR) that could be monitored. The P, I, and D settings would yield a modulation signal (MOD) which was multiplied to the RF signal driving the AOM with the help of a mixer.

3.2 Laser system

This section recaptures the stability requirements for the lasers and discusses possible implementations with one and two external cavity diode lasers (ECDL). As elicited in the theory chapter EIT is an effect that involves three electronic energy states and two light fields. Two of the energy states have to have a long decoherence time. These are also the levels where one laser field each starts and are connected via the third state. Depending on the relative location of the fields one distinguishes between Λ-, V- and ladder-type EIT. In this work Λ-type EIT connecting Zeeman sub-levels and Λ-type EIT connecting hyperfine ground state levels in ^{87}Rb has been investigated. (Other schemes like ladder-type or V-type EIT or coherent phenomena involving more than two light fields (e.g. tripod schemes) have not been investigated.) Therefore two light fields need to be sourced. This section discusses how to produce these fields.[1]

[1]Using the different words "beam" and "field" is an attempt to emphasise their different character, namely that "beams" occupy different spatial modes and can be physically deflected and routed over the laser table whereas "fields" can also occupy the same spatial mode while only differing by polarisation and/or in frequency. In addition, "fields" that occupy the same spatial mode are also not easy to manipulate separately in time (c.f. the concatenated AOM and EOM in Phillips et al.[52]). Similarly, the expressions probe beam and control beam might be shortened to just probe and control at times.

3.2.1 The External Cavity Diode Lasers

The laser systems used for this thesis were two ECDLs from different companies (Toptica Model DL-110 and *MOGLabs* EDC-003). Single mode laser diodes for 795 nm (D_1 line) and 780 nm (D_2 line) were sourced from LaserComponents. In the beginning of the project there was only the *Toptica* laser since the second laser had not been bought yet. This limited the investigations to Zeeman schemes. The *Toptica* had been ordered with a laser diode for D_2 because the atom-cavity system runs on the D_2 line and it was thought that EIT would work equally well in a Zeeman scheme on D_2. This was the reason why investigations started with the Zeeman scheme on D_2. The second laser was only bought a year later and was actually supposed to be used as another laser in the atom-cavity project but was then made available for the EIT project when it became clear that hyperfine schemes need to be investigated.

The timeline was as follows: In the beginning only one laser was used at 780 nm to investigate Zeeman schemes on the D_2 line by splitting the laser into a probe and a control beam. When the second laser became available with a laser diode for 780 nm, investigating hyperfine schemes on the D_2 line was possible by using one laser each for probe and control.

Then, one of the laser diodes was changed to 795 nm which enabled investigating Zeeman schemes on the D_1 line. Finally the second laser diode was also changed to 795 nm so that hyperfine schemes on the D_1 line could be investigated.

3.2.2 Comparison of Toptica and Moglabs ECDL

The two lasers both use the same method of grating feedback (the popular Littrow configuration in which the -1 order of a blazed reflection grating provides external feedback to the laser substrate). The *Toptica* laser features a brass mount with a virtual pivot point for the grating, the *MOGLabs* has its grating directly glued onto a piezo and therefore does not make use of

additional pivoting. The piezo itself is glued to a simple Thorlabs kinematic mount. The expected mode hop-free tuning range (MHFTR) should be higher for the *Toptica* (which it is), but the *MOGLabs* was able to routinely achieve a MHFTR of 10 GHz which is sufficient for full spectral scans of the Rb D lines.

The lasers differ vastly in the maximum value for the grating scan frequency. The *Toptica* grating controller provides a scan frequency up to several kHz whereas the *MOGLabs* in the original design only provides up to 8 Hz because the current driver in the HV module can not provide higher voltage swings. Triggering an analog oscilloscope on such a slow oscillation (slower than the $\sim$25 Hz eye response) leads to severe flickering of the displayed traces on the oscilloscope screen and can be incredibly uncomfortable to the eye after a while. [2]

The *MOGLabs* laser diode and the grating sit in a solid aluminium trough. To access the collimation lens tube the lid needs to be removed and it was found that putting the lid back in place misaligned the feedback slightly. The mirror mount horizontal and vertical alignment screws were accessible from the outside.

A slight disadvantage from a UK's point of view is that there is currently (2013) no European service center and sending the units for repair takes a considerable amount of time although *MOGLabs* turn-around time might be as short as one day. Although sending a part for repair might be as short as a couple of days, it is the UK Customs re-import and their communication with the physics department that can take a really long time (one to several weeks).

3.3 Possible laser field preparation

Several setup schemes are possible. What follows is an overview of different setups for the hyperfine and Zeeman-EIT schemes.

[2] Upon enquiry *MOGLabs* suggested replacing two SMD resistors on the main circuit board in order to achieve up to 30 Hz. Considering the risk of breaking things this modification was abstained from.

# lasers vs scheme	one laser	two lasers
Zeeman-scheme	beam split and independent preparation, EOM+AOM [52], same mode	possible but usually not necessary, PLL, injection seed
HF-scheme	GHz EOM or current modulation bias-T	PLL lock, GHz shifted injection seed

Table 3.1 Depending on what experimental scheme is run, the number of available lasers and the availability of other components, different laser beam preparation and locking schemes have to be pursued.

In the case of *Zeeman-EIT* one laser beam can be split into two parts by means of a beam splitter and henceforth the two parts can be independently prepared (beam shaping, polarisation, power, frequency, temporal switching) before recombining them on another beam splitter just before the Rb vapour cell. This method gives the most experimental freedom but will consume more components and can be cumbersome to achieve proper mode matching when overlaying the beams.

Without splitting the laser beam two fields can still be generated which is the route taken in the 2001 light storage experiment by Phillips *et al.* [52] where the experimenters attain the probe and control field from *one* laser beam by rotating the polarisation by a small angle so that in the HV basis (of the analysing beam splitter behind the vapour cell) there is approximately a 1:10 power distribution (probe to control) which gets converted into an equivalent ratio of σ^+/σ^- polarised radiation. Since an electro-optical modulator is used, both, constant generation of the probe field for EIT (due to the GHz carrier frequency of the EOM drive signal) *and* temporal shaping or pulsing (by shaping the EOM drive envelope) for slow light effects can be achieved this way. The fact that probe and control are here in the exact same spatial mode can be both an advantage and a disadvantage experimentally.

For *Hyperfine-EIT* two light fields with a frequency difference equalling the hyperfine ground state splitting of ^{87}Rb are needed. This frequency difference of 6.8 GHz is usually not trivially attained. There are several different methods to achieve this goal. And like above

one should distinguish between the ones which use only one laser and the ones which use two lasers.

In the case of *one* laser a straight-forward method is to create sidebands on the laser beam. This is either done externally by means of an electro-optic modulator [53] or internally by directly modulating the current of the laser diode [54].

Both of these methods though are not able to create only one additional frequency but they rather always create two new frequencies since sidebands always appear symmetrically. This immediately poses the problem of how to rid the unwanted sideband or, at least, leads to a discussion if the additional sideband is detrimental at all.

In some published experiments no filter attempts are made arguing that one of the two sidebands is far off resonance and has a negligible effect on the phenomenon that is investigated and can thus be neglected [55, 56].

Usually though, for better experimental control and avoidance of unwanted effects, like four wave mixing (FWM), experimenters try to filter out one of the sidebands while leaving the carrier and the desired sideband mostly unattenuated (e.g. as done in [9, 6]).

There are several ways for doing this. One possible implementation for filtering is to use filter cavities (etalons/Fabry-Perot filters) [57]. Another way is to use a Mach-Zehnder interferometer. A particularly nice implementation using two beam splitters and a right-angled glass prism has been done by [58]. Using the Faraday effect has been implemented in [59]. [3]

Another intriguing way would be to split off a beam and to shift it by means of AOMs. Though this sounds exaggerated for the ground state splitting of alkalis there are experiments that report using quadruple passing an AOM at a driving frequency of 1.7 GHz [60]. The overall efficiency might be small but this would just prepare the beam for being the probe or as

[3] What becomes evident here is that the problem of *"Filtering light fields that are a couple of GHz apart"* shows up as a challenge in different places in the research area of Atomic & Laser Physics.

an injection seed for a second laser if more power is desired.

All of these methods have in common that the relative phase stability of the lasers follows directly the stability of the micro wave source used for the modulation. Also, all but one of the methods create the frequencies in the same spatial mode.

In case of using *two* independent lasers that are to be stabilised to a frequency difference of 6.8 GHz there is a variety of different locking methods available:

- lasers independently locked onto Doppler-free pump-probe spectroscopy
- EIT offset lock ([61])
- phase locked loops (PLL) in different variations
- injection seeding with frequency shifted auxiliary beam sourced from master laser

3.3.1 Frequency locking

As can be seen from Fig. 2.2, the probe absorption minimum is closely located around the frequency of the control. Thus, it is important that the relative frequency difference between the probe and control laser beams (the two-photon detuning) is zero. Less critically, the control frequency (single-photon detuning) should be stable.

How this is achieved depends on the type of Λ scheme implemented. In the Zeeman scheme, the easiest approach is to take both beams from the same laser. However, if the ground state levels are different hyperfine levels, then the frequency difference between the probe and control is $\sim$6.8 GHz. A single laser could still be used, if its current is modulated at 6.8 GHz [54] or it has its frequency shifted by an electro-optic modulator. Here, two individual lasers were used. The simplest approach to frequency locking in this case involves stabilising the lasers independently using two separate rubidium cells. The disadvantage with this is that both drift independently around the locking point with a typical laser linewidth of 1 MHz, which can be

reduced by carefully tuning the feedback settings. An alternative approach which was briefly investigated was to lock one laser to its reference cell, and then induce an EIT transparency peak in the second laser's reference cell to which that second laser could be locked to. This feature would not only give exactly the ground state splitting, but would drift with the first laser, minimising the extent of relative frequency drift of the two lasers. Bell *et al.* [61] found that a spectral width in the beat note of less than 1 kHz was achievable with this approach. It was possible to induce such a feature in the *Toptica* reference cell on the D_2 line and use the *Toptica*'s electronics to generate an error signal, indicating that such a technique is viable with this equipment.

3.3.1.1 Saturation spectroscopy

Frequency stabilisation is conducted relative to a reference frequency. Here, since the desired frequencies were the transitions between energy levels of ^{87}Rb, the reference frequency was most conveniently provided by the absorption peaks in a rubidium vapour cell. In a gas, atomic movement causes a Doppler broadening of the peaks, making these unsuitable as a frequency reference. Instead, a Doppler free spectroscopic method is used. A full exposition of Doppler free spectroscopy can be found in [35, p. 156]. A strong pump beam and a weak probe beam of the same frequency counter-propagate through a Rb vapour cell. For those atoms with zero velocity along the beam axis neither beam will be Doppler shifted. Suppose the frequency is scanned across a transition. Then, the pump beam will move atoms out of one hyperfine ground state into the other hyperfine ground state by means of hyperfine optical pumping [62], and so the probe will encounter fewer atoms to interact with at that frequency, giving rise to a series of transmission peaks visible in Fig. 4.2 and labelled F and F'. If two or more transitions lie within each others' Doppler profiles, additional 'crossover' peaks will occur, at a frequency half way between the two transitions. For this frequency, there exists a class of atoms which will see

the pump frequency red shifted onto the lower frequency transition, and the probe blue shifted onto the higher frequency transition. The pump will still depopulate the ground state, and so the probe will experience a peak in transmission. These are visible in Fig. 4.2 (labelled $C_{i/j}$) and can also be used as locking points.

3.3.1.2 Laser locking

The peaks generated by saturation spectroscopy still need to be turned into an error signal before they can be fed back to the laser. Such a signal is zero at the locking frequency, and has a slope such that if the laser frequency drifts to either side of the locking point a change in voltage to the piezo shortens or lengthens the cavity slightly, or adjusts the current, to correct for the drift. There are many different laser locking methods; The *Toptica* laser operates with a Pound-Drever-Hall technique. This produces frequency sidebands at $\pm$20 MHz which also pass through the rubidium cell. Electronic processing of the photodiode signal generates the error signal. The disadvantage of this approach is that the sidebands carry through to the experimental system. In contrast to this the *MOGLabs* laser modulates the external frequency reference at 250 kHz with an oscillating magnetic field. Both lasers are equipped with a proportional-integral-derivative (PID) feedback system to allow the error signal to be used to correct for both long term and short term drifts.

To test the linewidth of the lock, one laser was locked to the $C_{1/3}$ peak and the other to the $C_{2/3}$ on the D_2 line, both beams were shone onto a fast photodiode (bandwidth 150 MHz) and the resulting beat note was measured, shown in Fig. 3.6. The measured FWHM of the central peak in frequency space is 610$\pm$10 kHz, giving an average linewidth for each laser of 430$\pm$7 kHz, assuming equal contributions of the individual laser linewidths to the root mean square line width of the beat note. The location of the peak is 81.5$\pm$0.2 MHz, and the two smaller peaks corresponding to the frequency sidebands can be seen at 61.4$\pm$0.2 MHz and

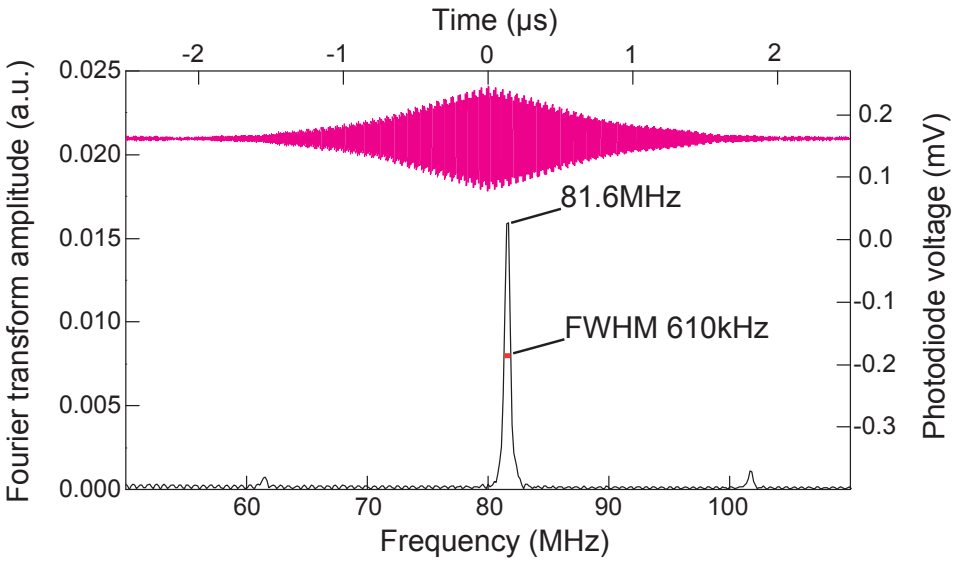

Figure 3.6 A beat note (top) and its Fourier transform (bottom) observed between the *Toptica* laser locked to $C_{1/3}$ peak and the *MOGLabs* laser locked to $C_{2/3}$. The plot is averaged over 500 traces. Due to this averaging the beat note is a bead since all the traces triggered to a rising slope are aligned at time zero and frequency deviations start to average in a destructive manner at a time difference equal to the inverse of the line width.

101.5±0.2 MHz. The relative location of the sideband peaks is as expected, but the central peak is not the calculated frequency difference of 78.5 MHz. This is probably because of a slight offset in the error signal. This linewidth is of the same order as the EIT linewidth, and so may well cause additional distortion of the peak [63].

3.3.2 Control of beam direction and polarisation

In the investigation of EIT, it was paramount that the polarisation and orientation of the coupling and probe beams be as well-controlled as possible: an angular deviation of even 0.5 mrad, equivalent to a separation of 0.5 mm after a beam length of 1 m, would cause a reduction in transparency of over 50% [64], and orthogonal polarisations were required in order to be able to filter the beams once they had propagated through the experimental cell. Also, in the Zeeman scheme, orthogonal circularly-polarised beams were required in order to access the relevant atomic transitions (see Fig. 5.2(a)).

Before assembling the experimental setup all optical components were aligned to work best

on a 5 inch beam height. With the help of an optical needle an auxiliary beam that went once around the optical table was adjusted to precise height. Then, using this beam and the needle all mirrors, polarising beam cubes, non-polarising beam cubes and lenses would be aligned to keep the outgoing beam on 5 inch beam height. This prior alignment routine helped to reduce the time needed to achieve good vertical overlap of beams where required. Over 5 m beams would deviate by a maximum of ± 0.5 mm. Initial vertical angular deviation of mirrors and beam cubes could thus be aligned to ± 0.1 mrad. This way most beam walking needed only to be done in the horizontal plane.

Single-mode non-polarisation maintaining optical fibres were used to guide laser beams from the beam preparation to the experimental setup. By making loops in the fibre the output polarisation could be controlled and thus maximised to take on the desired polarisation. A standard commercial three-loop controller had not been purchased. To produce a self-made controller in the machine workshop was considered too time-consuming at that point in time. Since optimal radii for the loops were not known [65] the fibre was at first arbitrarily looped and taped to the optical table. Whilst monitoring the output of the fibre behind a polarising beam cube the fibre looping and twisting was altered until the desired polarisation was maximised and then fixed in that position.

3.4 PLL laser stabilisation scheme

The PLL stabilisation schemes found in the literature differ by the frequency range in which the phase comparison happens. In recent years a handful of groups reported on their individual PLL schemes (Appel *et al.* [66], Hoeckel *et al.*[67]). Where the scheme in [66] divides the GHz frequency down into the RF range with a PLL chip from *Analog Devices* this includes a self-made PCB design. The setup in [67] on the other hand does not divide the GHz beat frequency

but compares the phase directly in the GHz range. Since the former requires abundant DIY work and the latter involves more costly microwave components, in this work a cheap ready-to-use fixed-ratio frequency divider is used to translate the GHz MW into MHz RF. The divider is sourced from *RF-Bay* and they have a wide range of fixed divide ratios in an affordable price range.

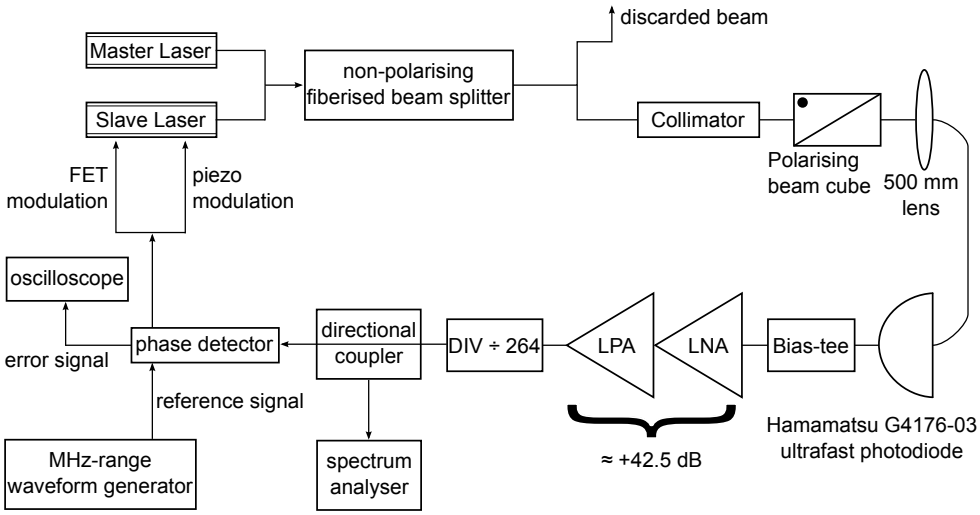

Figure 3.7 Here the *MOGLabs* is used as the master laser and the *Toptica* as the slave laser. An auxiliary beam of a few mW of each laser is split off and coupled into a non-polarising fibre beam splitter. One of the output ports is then illuminating a photodiode with 12 GHz bandwidth. A bias-T is used to apply a bias voltage to the photodiode and to extract the 6.8 GHz beatnote. The very low power of this signal made necessary a dual amplification (*RF-Bay* LNA-8G and LPA-7-25). The amplified signal is then given to the divide-by-264 divider. The divided down signal is then compared to an RF local oscillator with a phase detector or a mixer whose output port supports DC signals. The output of the phase detector is then used as a feedback signal on a fast path to the current of the slave laser and on a slow path via a PID regulator to the grating piezo of the slave laser.

Figure 3.7 depicts the experimental setup for the PLL. Two auxiliary laser beams, one each of the two lasers, are overlapped in a fibre beamsplitter. One of the beamsplitter outputs is collimated and directed to a focussing lens in whose focal point a high bandwidth (12 GHz) photodiode is located. The lens was mounted on a translation stage for better longitudinal alignment. The photodiode subsequently converts the optical beatnote of the two lasers into an electronic signal. Collimation of the beam and focal length of the lens are chosen so as to illuminate the active photodiode area as homogeneously as possible whilst minimising the

clipping. An unnecessarily small focus here will only risk damaging the photodiode. It should be pointed out that the beam waist should be experimentally verified (with a beam profiler or knife edge method) since relying solely on calculated values from datasheets can result in a very different (wrong) focus width. The maximum rating for the illumination of the photodiode is 5 mW when the square area of 200 μm $\times$ 200 μm is illuminated homogeneously. The photodiode is pre-biased[4] by a 9 V block battery through the DC port of a bias-T. The photodiode is manufactured onto an SMA connector and can therefore be easily mounted onto the combined RF & DC port of an SMA connectorised bias-T. The beatnote is extracted through the RF port. Since the electronic beatnote comes out in the region of -40 dBm at illumination powers of 2$\times$1.5 mW the fibre beamsplitter also helps maximising the contrast of the beatnote. In order to maximise the signal from the photodiode it was found that monitoring and maximising the current drawn by the photodiode while optimising the beam pointing is much easier than monitoring the RF signal on an oscilloscope. The next component in line would be the frequency divider but it specifies a minimum input power of -3 dBm[5] and a maximum of +12 dBm and therefore an amplification stage is used to make up for this power deficiency. An amplification between +33 dB and +52 dB was therefore needed. Since no commercial product was available working at 6.8 GHz and providing +40 dB amplification with an output power of 0 dBm two amplifiers had to be used. In this case RF-Bay amplifiers LNA-8G and LPA-7-25 were used with amplification values at 6.8 GHz of +17 dBm and +26 dBm respectively. Despite initial testing to check compliance with the datasheet one of these amplifiers (the one with the smaller amplification) broke soon and an interims solution has been found by replacing it with an amplifier from Minicircuits (ZX60-8008E+) that provided only +8 dBm. In this case it was

[4]The usual expression "reverse-biased" does not apply here as it is a MSM (metaloxide-semiconductor-metaloxide)-type photodiode *Hamamatsu* G4176-03.
[http://www.hamamatsu.com/resources/pdf/lsr/G4176E.pdf]

[5]Although it has also been proven to work at a typical input power of -7 dBm.

a lucky coincidence that the specifications in the datasheets of all the components involved so far were on the conservative side and that the setup with the replacement amplifier worked.

The frequency divider FPS-264-8 expects ∼0 dBm at its input, and outputs -5 dBm as a square wave. Its input frequency range spans 0.8-8 GHz and with its divide ratio of 264 the output RF range spans 3-30 MHz.[6] From this information a certain flexibility can be expected by changing the local oscillator frequency.

Next the divided down signal is compared with a local oscillator on a phase detector. Here it was envisaged to use a cheap fixed frequency crystal oscillator (XO) with oscillation frequency of 26 MHz but it turned out to be more flexible to use the existing arbitrary waveform generator (LeCroy Arbstudio). The crystal oscillator also required some external electronic components and designing this circuitry and handling the (only 5 mm by 3 mm big) XO turned out to be an unexpected challenge.

The output of the phase detector finally is proportional to the phase difference and can therefore be used as a feedback signal for the slave laser. The phase detector used is the ZRPD-1 from *Minicircuits* and it yields 7 mV/degree and a maximum peak-to-peak voltage output of 1.8 V. Thorough study of the application notes of Minicircuits [7] regarding phase detectors reveal two things:

1. The output impedance is 500 Ω and not 50 Ω. This is by design in order to improve slope efficiency.
2. Square inputs are acceptable since sine waves are squared up internally due to phase detectors being doubly balanced mixers operated in saturation.

The first point in particular puts a dent into the nice setup as there was no straight forward way to buffer the 500 Ω output into high impedance and then impedance match into 50 Ω.

[6] data sheet: http://rfbayinc.com/productspdf/product308.pdf
[7] application notes: http://www.minicircuits.com/app/AN41-001.pdf

Several attempts to build a self-made impedance matching box using an opamp only led to additional excessive noise. Eventually the only feasible solution was to directly connect to the 50 Ω input of the fast current control at the expense of losing half the signal strength and potentially acquiring additional noise due to back reflections.

The second point raises the question if within the 264 oscillations that the GHz signal does to produce one oscillation of the divided down signal there could be phase fluctuations that stay "undetected" by the phase comparison in the RF range (see Figure 3.8).

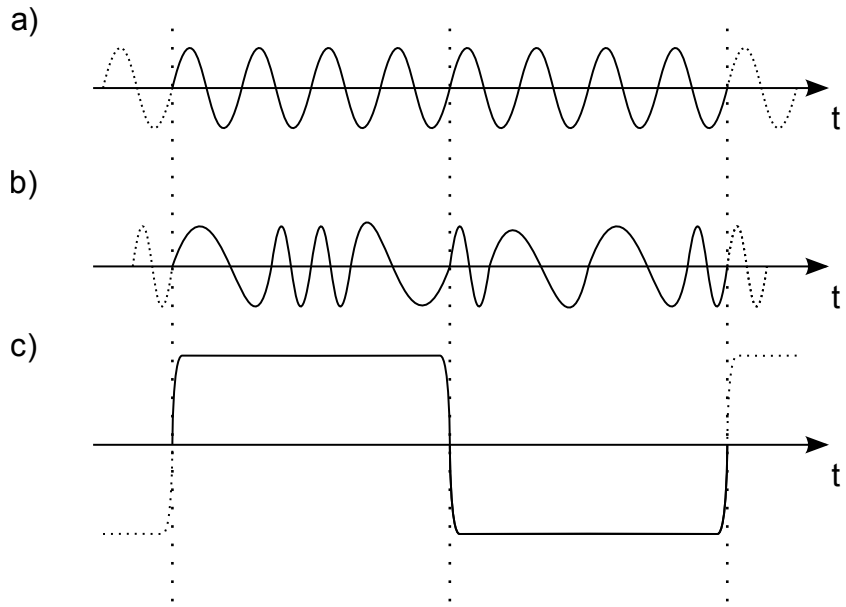

Figure 3.8 Shown are two signals that would lead to the exact same output of the frequency divider. One is nice monochromatic sinusoidal signal, the other a signal with additional phase noise. Since the noisy signal has exactly the same number of oscillations as the clean signal and the correct phase at the zero crossing of the frequency dividers output steps this additional noise could stay undetected.

From the *Toptica* manual it can be seen that around zero applied voltage the delta current is approx. 8 mA/V applied voltage to the current control FET. For small voltage changes the current change can be approximated linearly. Although it should be pointed out that the overall dependence is quite curved (see *Toptica* manual, p.32 and Fig. 3.10).[8]

[8] "Toptica DL 100 Laser Head Manual M8 Ver1 (21.3.06)", unavailable online.

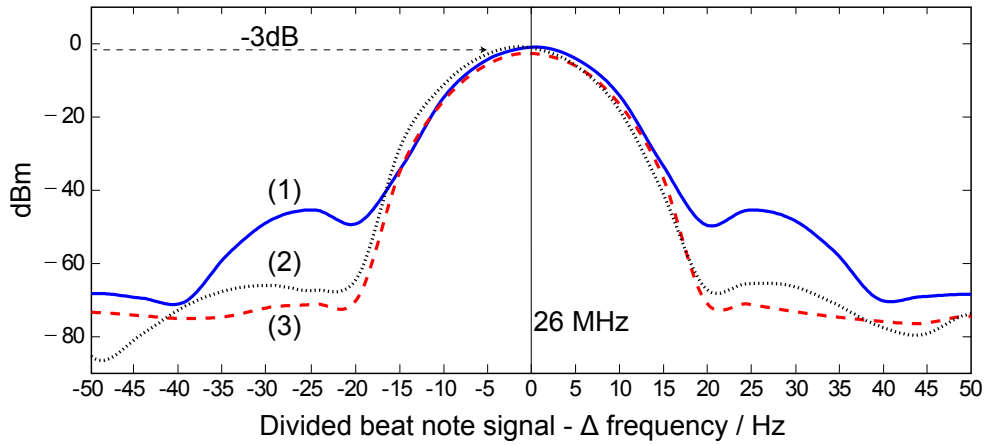

Figure 3.9 Power spectrum of the divided down beatnote in different closed-loop conditions. Plots: (1) With only the fast current feedback (blue solid), (2) with additional grating feedback (grey dotted line), and (3) after further optimisation of the PID parameters (red dashed line). The side-bands in trace (1) at 25 Hz are the grating scan that cannot be fully turned down (Toptica Electronics rack). Measured with spectrum analyser Agilent E4405B, centre frequency: 26 MHz, span: 154 Hz, resolution bandwidth (RBW): 10 Hz, video bandwidth (VBW): 10 Hz.

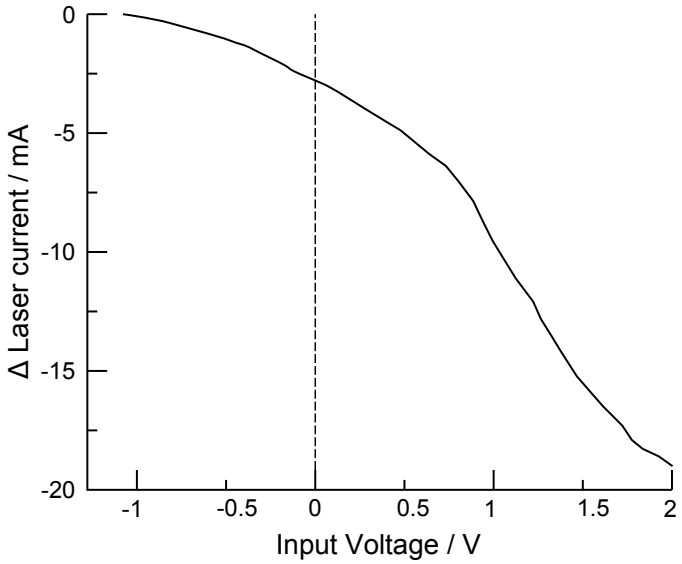

Figure 3.10 Bias-T control voltage to laser current modulation conversion for negative laser diodes. Coarsely depicted from *Toptica* Laser Manual.

The closed-loop divided beat was analysed by using the split off signal of a directional coupler. Though commercially available a directional coupler for the undivided beatnote at 6.8 GHz was not at hand in the lab.

The second output of the fiberised beamsplitter would be useful for diagnostic purposes. This has not been pursued as the necessary components, especially a second GHz bias-T, were not available at that time. Of particular interest would have been to examine the original GHz beat note and its linewidth.

After designing the physical implementation of the PLL circuit fine tuning of the feedback paths, characterisation of the setup and measurement of the residual linewidth was due.

The divided down signal measurement is limited by the resolution bandwidth of the spectrum analyser and has to be assumed to be 10 Hz wide. This means that the undivided signal could be up to 2.64 kHz wide.

Looking at the phase noise is a method of characterising the lock. Comparing the divided down beat note with a reference signal from an AWG it was found that the phase noise was distributed with a standard deviation of 1.15° or 0.02 rad. This phase noise is 264 times smaller than the true phase noise from the undivided beat signal. Multiplying $1.15^\circ \times 264$ gives a standard deviation of 304°, one cannot be sure that this will be the case for the undivided beat signal – in fact, it appears to be very unlikely. However, one can note that as an upper bound it is within one oscillation though it equals 5 radian. Other experiments that do not divide the GHz beat report phase variance errors of $0.02\,\mathrm{rad}^2$ [67] and $0.08\,\mathrm{rad}^2$ [66] or, equivalently, 0.14 rad and 0.28 rad for their standard deviations.

The lock was stable against the usual noise in labs (door slamming, talking and dropping light object onto the laser table.

Taking into account the operating ranges of all the involved components this PLL should

work in the range of 1–8 GHz and therefore provides a certain flexibility. Due to the dividing and phase comparison in the RF and the resolution bandwidth (RBW) of the spectrum analyser used the upper bound for the residual linewidth of the beatnote of master and slave is in the kHz range. The lock proved to be stable over extended periods of time (several minutes to hours).

An exhaustive characterisation and benchmarking of the lock would have included measuring time traces of different length and converting them into Allan variance data (as done in [66]). With this phase lock some EIT traces have been measured to compare this data to the unlocked case. Slow and Stored/Retrieved Light have not been attempted due to time constraints but should be greatly facilitated with a phase lock.

In a future setup one should use the method of injection seeding for the lasers. Shifting an auxiliary beam in multiple passes and then injecting it into a second diode laser would create the second field. The seeded laser would then amplify the frequency shifted beam to provide more power. But since all the experiments in this project only require a weak probe beam with a power in the μW range, it might, in fact, be enough to only shift a beam without optically amplifying it any further. Several reports on multiple pass AOM frequency shifting can be found [60, 68]. With the AOMs of 80 and 110 MHz centre frequency available here, this method is bound to fail as on the order of 50-100 passes are necessary. Both techniques for multiple passes, vertical displacement and polarisation change, are not known to have been successfully applied for more than 8 passes. Therefore a suitable AOM with centre frequency 1.7 GHz for quadruple passing or at 850 MHz for two consecutive quadruple passing stages would need to be purchased. Of course also an RF/MW source at that frequency is needed.

Chapter 4

Vapour cell characterisation

Contents

Every experiment starts with a proper characterisation of the involved components and used equipment. This is also to confirm the validity of the theoretical model and to figure out its parameters. With respect to the rubidium vapour cells the simplest experiment is a weak beam continuous wave spectroscopy. Figure 4.1 shows the setup for the single beam spectroscopy (at times also referred to as "standard spectroscopy").

4.1 Vapour cells

Several different mixtures of rubidium isotopes and buffer gases were investigated, to ascertain which factors dominate in EIT. Four cells were used: three cells with rubidium and buffer gas, and one standard cell with rubidium in natural abundance (72.2% ^{85}Rb and 27.8% ^{87}Rb [69]) and no buffer gas.

The vapour cells containing ^{87}Rb were acquired in the following order: natural abundance cells, cell with 40 Torr neon, cell with 10 Torr neon approximately a year apart. First EIT signals were attempted with the natural abundance cell which yielded some small signals (without data)

Cell	Rubidium isotope	Buffer gas	Length
1	^{87}Rb (99.9%)	10 Torr Ne	150 mm
2	^{87}Rb (99.9%)	40 Torr Ne	150 mm
3	^{85}Rb (99.9%)	120 Torr N_2	150 mm
4	Nat. Abundance	None	75 mm

Table 4.1 Overview of the vapour cells used in this thesis. The isotopically enriched cells were all specified to 99.9% although the real values turned out to be considerably lower (c.f. Section 4.2.2).

on the Zeeman scheme on the D_2 line and then finally in the Zeeman scheme on the D_1 line. The natural abundance cells were also used to provide a frequency reference for locking the external cavity diode lasers.

The isotopically enriched cells including the buffer gas were expected to yield experimental data for EIT and slow light and envisioned to be used in a later single photon storage experiment. These cells were ordered with antireflection-coated, wedged, and angled windows in order to rule out any back-reflections from or Fabry-Perot effects within the entrance and exit windows. The cells were also placed inside a triple shield made from mumetal.

Chiefly investigated was EIT in cell 1. There were other smaller cells containing rubidium in natural abundance which were used for well-characterised spectroscopic control of the lasers. The two glass windows in each cell were anti-reflection coated, to prevent back-reflections resulting in extended-cavity effects [70]. Despite the low reflectivity, the cells were mounted at a slight angle to the beam path, as an additional preventative measure. When in use, the experimental cells were placed inside a triply-shielding container made out of μ-metal—a nickel-iron alloy with a high magnetic permeability—in order to shield the cells from external magnetic fields. Such shielding was especially important when the Zeeman scheme was investigated: a static magnetic field lifts the degeneracy of the substates on each hyperfine level [35, ch. 6]. The setup used to characterise the cells is displayed in Fig. 4.1.

The laser scans across frequency by having a triangular voltage $V_p(t)$ applied to a piezoelec-

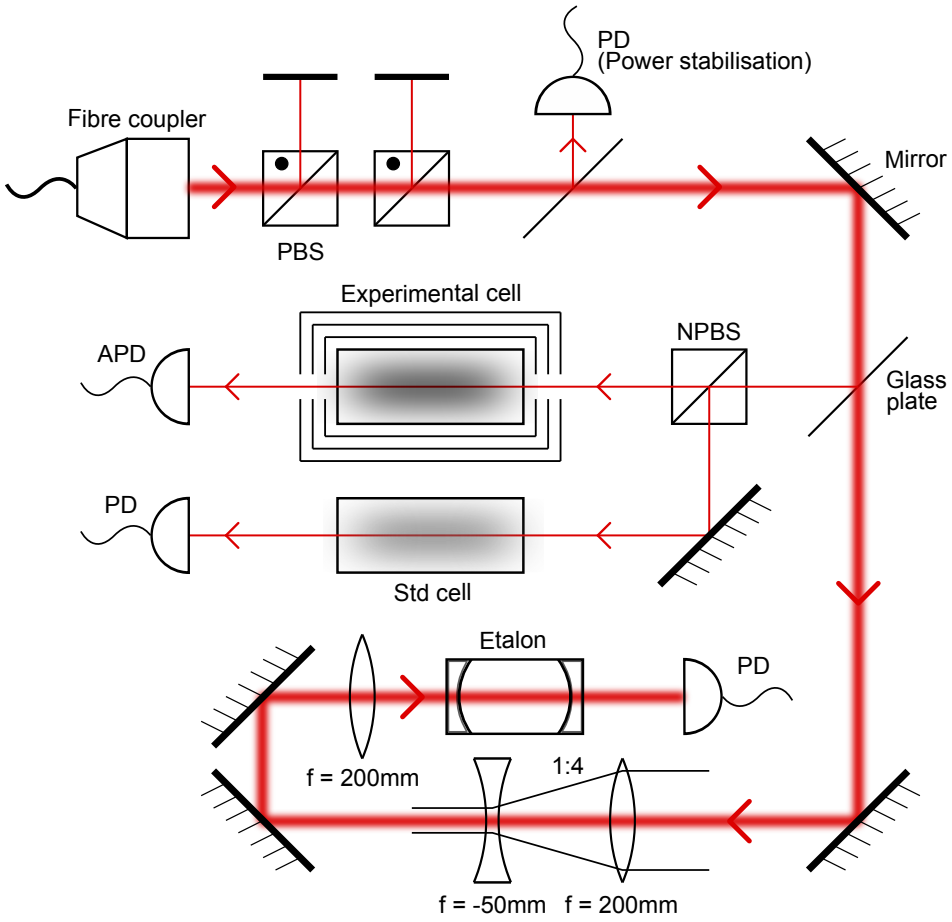

Figure 4.1 The setup used to measure the D_1 and D_2 absorption lines for different vapour cells at different temperatures. A laser beam is coupled out from a fibre coupler passing through two polarising beam splitters to ensure high polarisation purity. The power is monitored and fed into a PID regulator that alters the RF power of an AOM before the fibre, thus ensuring constant power while scanning the laser over the whole Rb D line. The beam is split into three beams: one for the cell under scrutiny, one for the Fabry Perot whose transmission peaks serve as frequency markers, one is for a Doppler-free reference spectrum. In an earlier version of this setup (without power stabilisation), a fourth beam would monitor the incoming power as this would change due to the current feed forward while scanning the laser grating. The power through the experimental cell was kept at 0.1% to 0.5% of the saturation intensity ensuring a "weak" probe [71].

tric element on the mounting of the laser's diffraction grating. The lasing frequency is roughly linear in $V_p(t)$, but to calibrate the frequency axis more precisely on the spectroscopic scans, part of the initial beam was coupled into a Fabry–Pérot etalon [72, ch. 9], where a photodiode measuring the output of the etalon would see sharp peaks in power at 750 MHz intervals. Imposing this interval as equidistant the frequency axis of the scans was linearised to make the etalon peaks equidistant.

Another part of the initial beam was diverted to a photodiode, for power stabilisation. As the piezo's voltage varies, a proportional part of this voltage (feed forward) leads to a change in the laser diode current, designed so that the dominant internal mode of the laser's gain medium is well-matched to the external mode, increasing the MHFTR. This change in current leads to a change in power, so requires a power stabilisation.

4.2 Spectroscopy

4.2.1 Doppler-free pump-probe spectroscopy

A standard method for resolving resonances that are usually merged with neighbouring resonances due to Doppler broadening is counter-propagating pump-probe spectroscopy. In this setup, a transmission spectrum will show additional features (mostly peaks but under special circumstances dips can appear on certain resonances) that reveal the location of the natural resonances. In the weak probe limit these will show and are only limited by the natural line width. The lasers have been routinely locked onto these Doppler-free resonances using frequency modulation. Fig. 4.2 shows both D lines for natural abundance Rb for Doppler-free pump-probe spectroscopy.

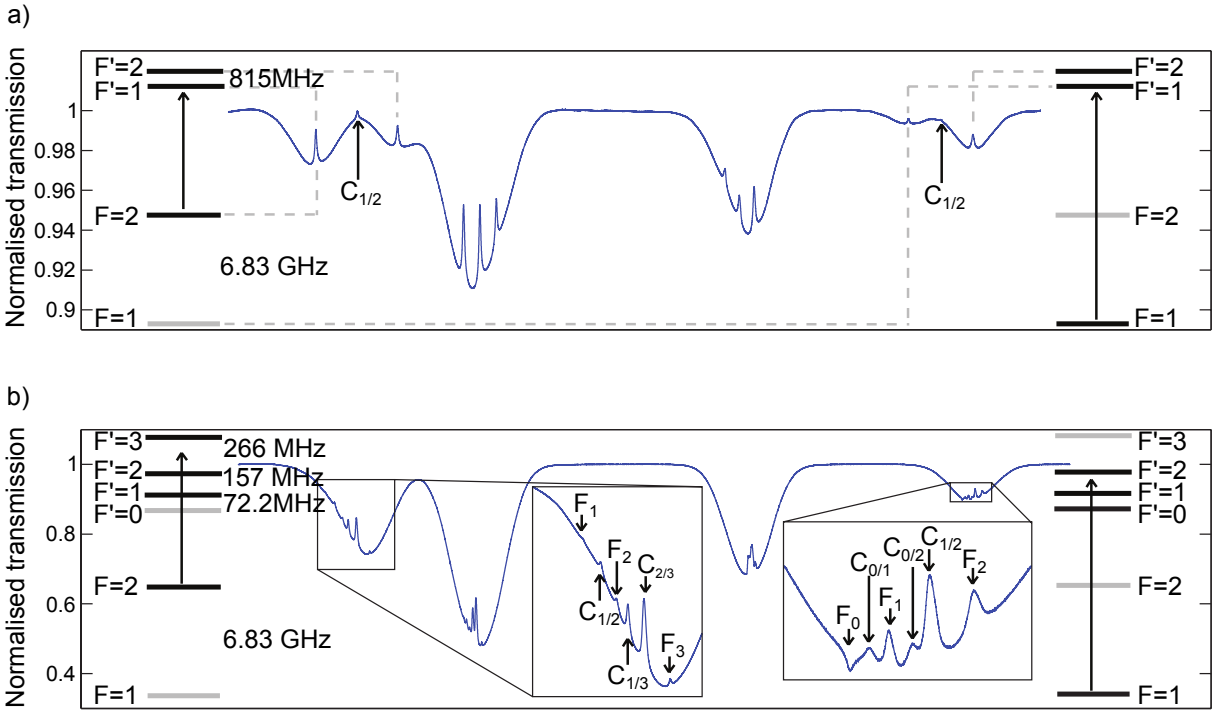

Figure 4.2 Doppler-free saturation spectroscopy of the D_1 (top) and D_2 (bottom) lines of Rb, taken at room temperature for a cell with natural Rb of 75 mm length, 1024 traces averaged. The two dips on each plot closest to the centre correspond to ^{85}Rb and the outer two to ^{87}Rb. The series of peaks on the left hand side of each plot correspond to the transitions starting at F=2, and on the right hand side correspond to those starting at F=1. Levels which are inaccessible to the probing laser because of the selection rules are shown in grey.

4.2.2 Vapour cell characterisation with a weak probe

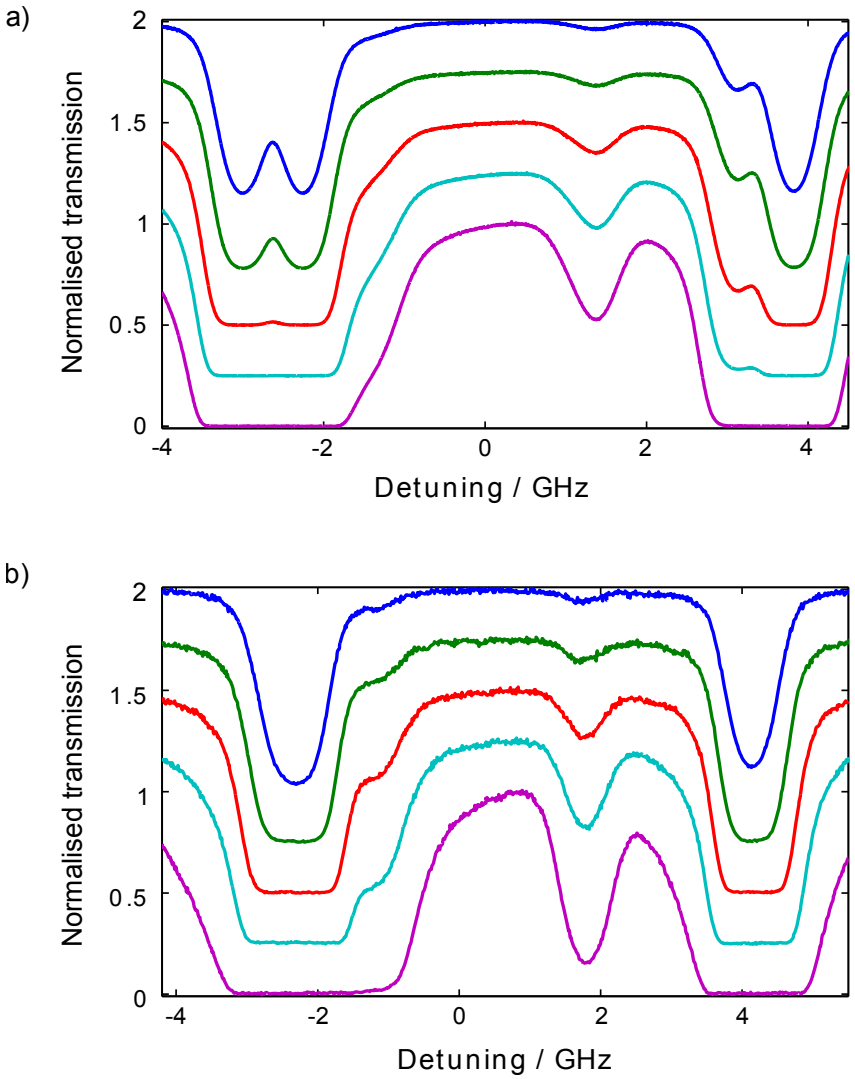

Figure 4.3 Spectroscopy of cell 1, about the D_1 (top) and D_2 (bottom) absorption lines, where zero detuning is defined at a "centre-of-mass" frequency: where the absorption line would occur in the absence of hyperfine splitting, weighted according to the natural abundance of each rubidium isotope [69]. 0 to 1 corresponds to transmission of 0 to 100%, except that each curve is successively offset by +0.25 units vertically, for clarity. In the D_1 scans, the cell was at temperatures of, from top to bottom, 34.0, 40.8, 50.6, 58.5, and 67.2°C. In the D_2 scans, the temperatures were, from top to bottom, 27.0, 36.2, 45.6, 54.7, and 70.0°C.

The cells were illuminated with approximately 800 nW of light, with a 3.5 mm beam diameter, giving an intensity of 0.083 μW/mm^2, which is 0.5% of the saturation intensity, I_{sat}=16.7 μW/mm^2 [73].

Figure 4.3 shows the spectroscopy data of cell 1 for various temperatures. The two features on the left-most side of the D_1 scans are due to the transitions from the ground state F=2, and on the right-hand side, the F=1 transitions. On the D_2 scans, due to small hyperfine spacing in the $5^2P_{3/2}$ manifold and their relative differences in absorption strength, the F=2 transitions appear as a single dip in transmission on the left-hand side, and similarly for the F=1 transitions on the right-hand side. The dips near the centre of each scan are due to a residual concentration of ^{85}Rb, betraying an isotopic purity of less than 99.9% in the cell. A detailed treatment of Doppler-broadened absorption on rubidium D lines is available in Siddons et al. (2008) [69].

The scans were found to be in good agreement with the model described by [69], in which the pressure broadening according to [48] was phenomenologically added as a broadening of the Lorentzian natural line width, which underlies the Voigt profile (a convolution of Gaussian and Lorentzian lineshapes) [35] (see Fig. 4.3). Increases in temperature would lead to greater optical depths (OD=$\alpha(\omega_p)L$). This caused the transmission about the resonances in each rubidium isotope to uniformly level out at zero at temperatures of 55°C.

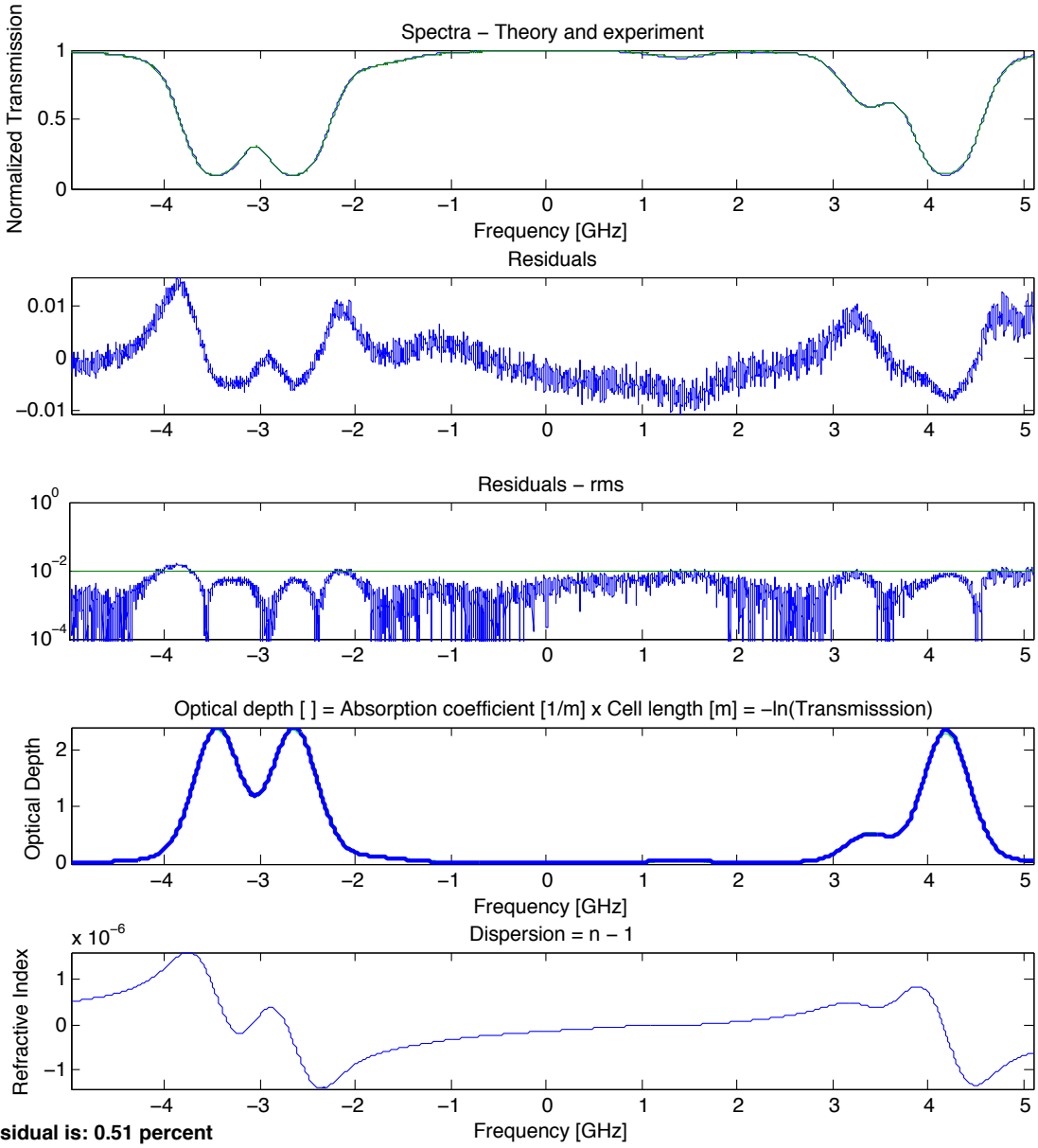

Mean residual is: 0.51 percent
Opt temp is: 308.3 Kelvin or 35.2 +/– 0.5 Celsius.
Opt freq is: –0.429 GHz.
Rb–87 fraction is 98.03 +/– 1.26 percent.
Opt freq is: –0.429 +/– 0.017 GHz.

Figure 4.4 Shown here is a typical evaluation plot for fitting the adapted absorption model to measured data. The cell parameters are L=15 cm, 10 Torr neon, D_1 line. The first plot shows data (green) and best fit (blue). The second plot shows their difference, called residuals. The third plot shows the absolute value of the residual on a logarithmic scale. The green line indicates the 1% level. The fit routine minimised the overall sum of the square of all the residuals. The fourth plot shows the negative logarithm of the measured data and the absorption coefficient from the model. The fifth plot shows the calculated dispersion.

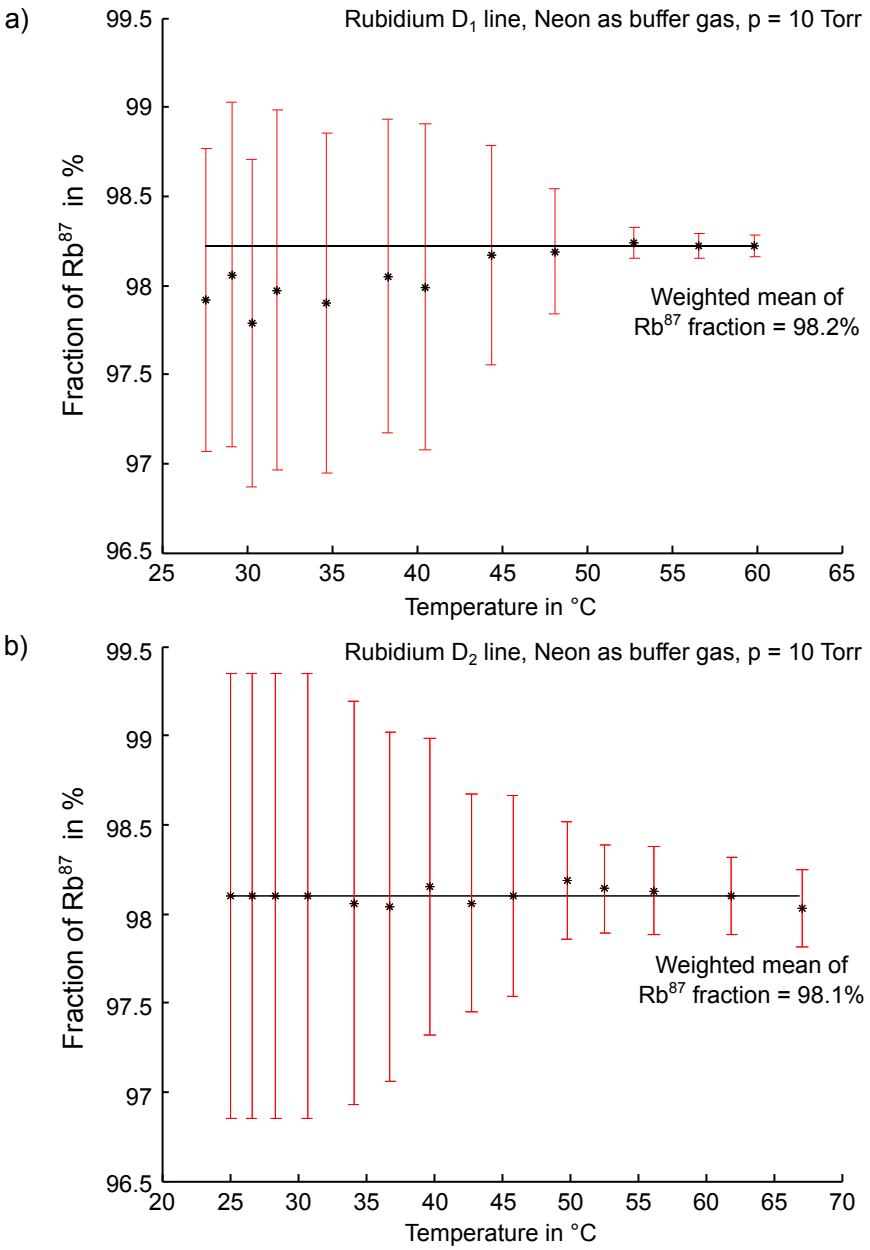

Figure 4.5 Plotted are the different best fits of the isotopic fraction of ^{87}Rb at different temperatures including error bars. There is no functional dependence. The horizontal axis could also be titled "# of measurement". But clearly seen can be the trend that for higher temperatures the error bar gets smaller. The horizontal line is the weighted mean. This series of measurements and fits proved that the vapour cell supplier did not meet their own specified value of "better than 99.9%".

Chapter 5

Electromagnetically induced transparency

Contents

5.1 Setup for electromagnetically induced transparency

Figure 5.1 shows the setup that was used to investigate EIT, slow light, and storage and retrieval of light in the rubidium vapour. The mirrors and beam splitters are aligned such that, going into the cell, the probe and control beams are co-propagating and overlapping as much as possible. Before entering the cell, the control and probe beams are vertically and horizontally polarised, respectively, but if orthogonal circular polarisations was required in the cell, a quarter-wave plate could be placed before the cell.

Prior to entering the fibre-couplers, the control and probe beams each made a double-pass through an acousto-optic modulator (AOM). Signals applied to the AOMs were produced by an arbitrary waveform generator (AWG). The control AOM was driven with a constant frequency and intensity, whereas the probe AOM was either scanned with constant amplitude, causing a ± 2 MHz shift in probe frequency, or produced a sine-squared shaped pulse (with an underlying carrier wave), occurring at 5 ms intervals.

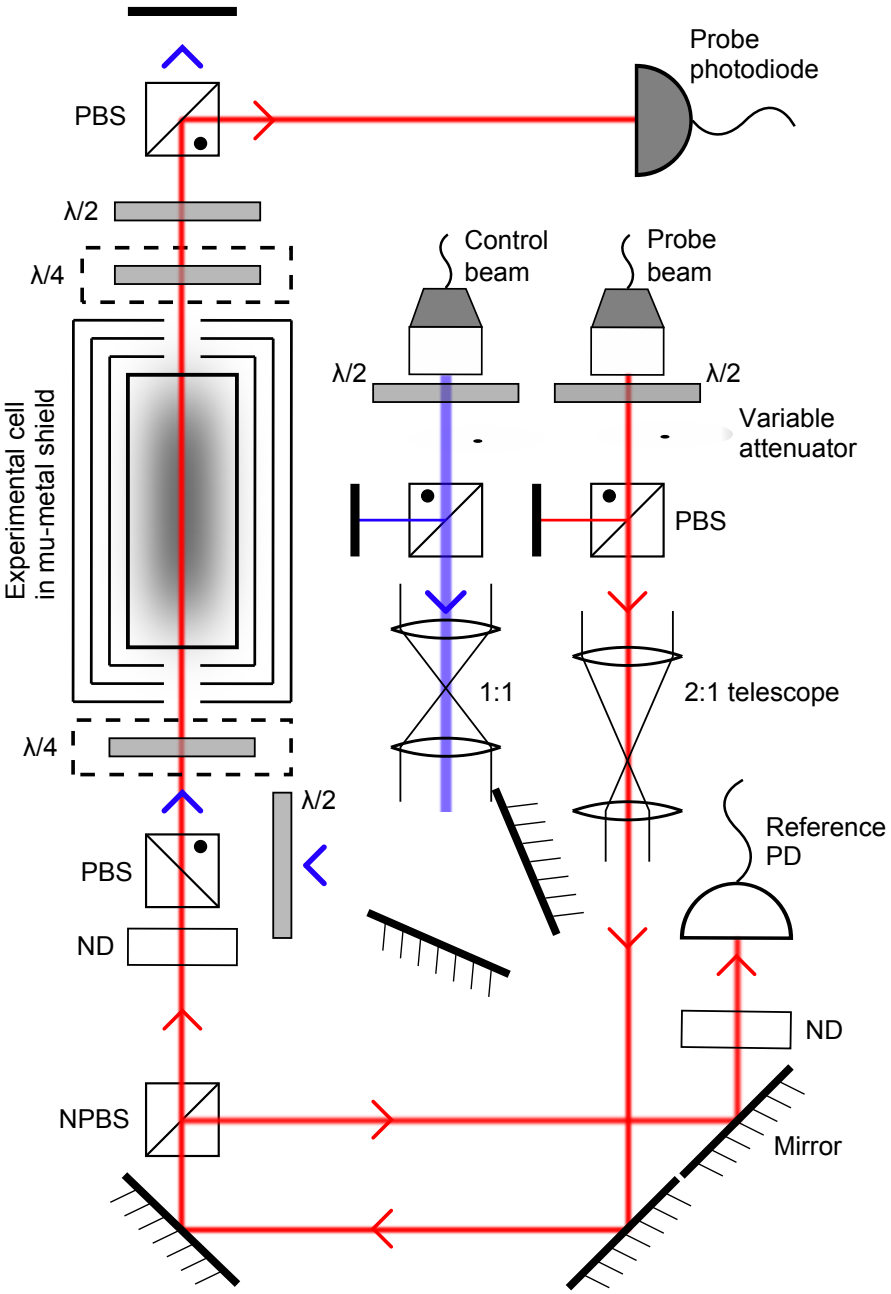

Figure 5.1 Experimental setup used for EIT and slow light and storage experiments. Control and probe beams are individually fibre-coupled and guided from the laser preparation stage to the experimental setup. Half wave plates and polarising beam splitters are used to maximise power in forward direction. Telescopes adjust the beam widths. Before overlapping the beams on a polarising beam splitter the probe beam is split into two beams two provide a reference beam for the slow light experiments. Neutral density filters (ND) are adjusted so that the photodiode signals of probe and reference can be displayed on an oscilloscope for immediate comparison.

Both fibre-couplers output a 3.5 mm-diameter beam. A telescope was placed in front of each fibre-coupler in order to optimise the collimation of the two beams, as well as to halve the diameter of the probe, so that the control beam was overlapping enough to appear sufficiently uniform to the probe[1].

The probe beam was split into two, the probe signal that would propagate through the cell, and a reference beam that would allow to ascertain where the 100% transmission level was, and also to give a zero-delay marker when working with pulses. The reference and signal arms of the setup were roughly the same length ($\ll 1$ m path difference), but even a difference of 1 m would result in a deviation of 3 ns from the true zero-delay, which was negligible compared to the pulse-delay observations.

EIT was investigated on two transitions[2] of ^{87}Rb, the D_1 line, $5s\ ^2S_{1/2} \rightarrow 5p\ ^2P_{1/2}$, and the D_2 line, $5s\ ^2S_{1/2} \rightarrow 5p\ ^2P_{3/2}$, with wavelengths of 795 nm and 780 nm respectively. The reason for considering two transitions stems from the compatibility requirements with the single photon source. In the single photon source, the cooling, trapping and manipulation of the ^{87}Rb atomic cloud in a magneto optical trap (MOT) requires laser beams (near) resonant to an atomic transition isolated from those transitions used for the V-STIRAP process. Therefore, either all lasers must be on the D_2 line which has sufficient levels in the $5p\ ^2P_{3/2}$ manifold, or the cooling and V-STIRAP beams must be on different fine structure transitions. Given that the single photon source was operating on the former scheme, investigation was started on the D_2 line. Since the nuclear spin of ^{87}Rb is 3/2, the terms undergo hyperfine splitting giving a range of states labelled by F and shown in Fig. 4.2. Further splitting of the hyperfine states into Zeeman states labelled by m_F is also possible by applying a weak magnetic field. This gives two classes

[1]Both beams had a Rayleigh length (length of propagation in which the beam diameter widens by a factor of $\sqrt{2}$) much greater than the length of the experimental cell (10 m and 2.5 m for the control and probe beams respectively), and as such, they were considered to be plane waves [74, pp.664-669].

[2]for a comprehensive guide to the properties of these transitions, see [47]

of Λ schemes: in Zeeman schemes different m_F states on the F=1 or F=2 line are used as the ground states $|1\rangle$, $|2\rangle$. In hyperfine schemes the different hyperfine levels F=1 and F=2 are used as the ground states.

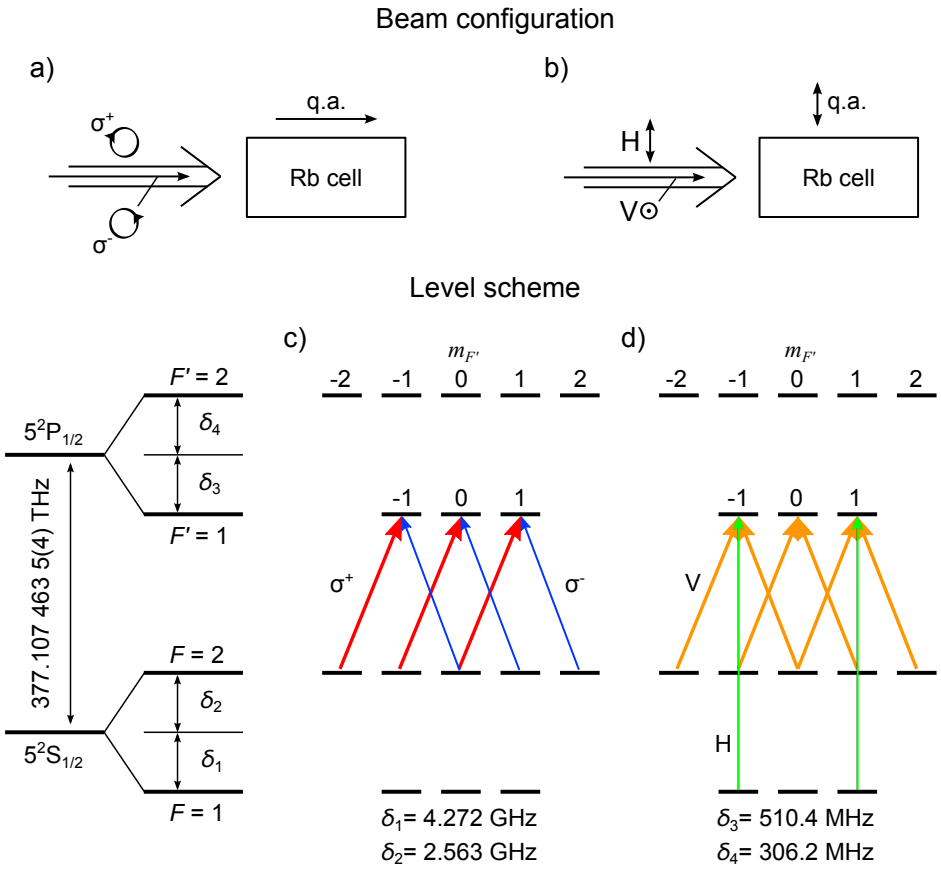

Figure 5.2 The Zeeman substates of the hyperfine levels on the ^{87}Rb D_1 line (duplicated for clarity). (a) shows the levels in the Zeeman scheme, with σ_+ control light (red), and σ_- probe light (blue). (b) shows the structure of the Hyperfine scheme. By choosing the quantisation axis to be parallel to the probe beam, the atoms see a linearly polarised probe (green), and a coherent superposition of σ_+ and σ_- control light (orange). Due to selection rules there is no absorption for m_F=0$\rightarrow m_{F'}$=0 on the F=1$\rightarrow F'$=1 transition.

The key features of the optical arrangements common to both schemes are shown in Fig. 5.1. In the Zeeman case control and probe beams are produced from the same external cavity diode laser whereas in the hyperfine case two different diode lasers are used. Each laser can be frequency stabilised relative to a reference rubidium cell or set to scan frequencies in a range up to $\sim$10 GHz. The beams are each double passed through separate acousto-optic modulators (AOMs) to enable power modulation and frequency shifting. Half-wave plates ensure that the

probe is horizontally polarised and the control is vertically polarised, before the beams are combined on a polarising beam cube, and aligned to give maximum overlap. The polarisation can be adjusted with a quarter and half wave plate before the beams are passed through a heated rubidium cell and another set of waveplates returns the probe and control polarisations to horizontal and vertical, respectively. Finally, a Glan-Laser polarising beam cube (measured suppression 1:11,000) removes the control laser, and the remaining probe laser power is measured with a photodiode.

A reference photodiode is also shown. This enables the intensity of the probe beam to be stabilised when conducting continuous wave spectroscopy of the EIT feature via a feedback loop to the AOM modulation voltage. When the laser is operating in pulsed mode, this photodiode provides a reference pulse against which the delay of light can be measured.

5.2 EIT Results

This section presents the EIT results in chronological order. Investigating a Zeeman scheme always preceded the investigation of a hyperfine scheme because probe and control field can be produced by one and the same laser. The D_2 line was investigated first since the Toptica laser was ordered to initially contain a laser diode for 780 nm.

5.2.1 Zeeman-EIT on D_2 line

There are no Zeeman D_2 results because no significant signals could be observed. Worth mentioning that this was the scheme initially envisaged for the whole project. This stems from the fact that the D_2 line provides one of the cleanest Λ arrangements of energy levels, namely F=1, $m_F = \pm 1$ and F'=1, $m_{F'} = 0$. The next neighbouring level in the excited state is -78 MHz away. While this provides a nice transition scheme for cold atoms, e.g. in the single photon

production process in an atom-cavity system, thermal ensembles due to their Doppler broadening will also provide the neighbouring possible energy schemes. This is detrimental for any coherent effect to build up, especially because the F'=0, $m_{F'}$=0 state has Clebsch-Gordon coefficients of opposite sign compared to the Λ system mentioned. Therefore one system's dark state is the other system's bright state. (I. Novikova pointed out this fact during a lab tour.)

5.2.2 Hyperfine-EIT on D_2 line

Investigations began by using a hyperfine scheme on the D_2 line. A variety of Λ schemes were tried, the results shown in Fig. 5.3 were for the following scheme: The control was locked from the F=2 to the $C_{2/3}$ peak, and shifted down 162.5 MHz by an AOM. The probe beam was set to scan in the region of the F=1 $\rightarrow$ F'=1 transition, and shifted up 162.5 MHz. This gave a two photon resonance 29.5 MHz below the F'=2 line. The control power was varied, and the probe power was set to 37 μW, both on a 2 mm beam diameter.

Initially it was attempted to use a high temperature, to give a medium which was opaque to the probe without the control being applied. However, this gave just 10% transmission, even with maximum control power.

Therefore, a lower temperature of 53°C was chosen and the series of EIT features at different powers shown in Fig. 5.3 could be observed. This figure shows that increasing the control power does increase the EIT peak size and FWHM as predicted by Eqns.(2.11) and (2.10), but it also increases the depth of the absorption dip in which the EIT feature sits, and so the medium actually transmits less light with stronger control.

By studying Fig. 4.2, it can instantly be seen that on the D_1 line the hyperfine splitting of the excited energy level is larger than the Doppler broadening of the peak (815 MHz vs. $\sim$500 MHz). In contrast, on the D_2 line the largest splitting is 267 MHz, so even at room

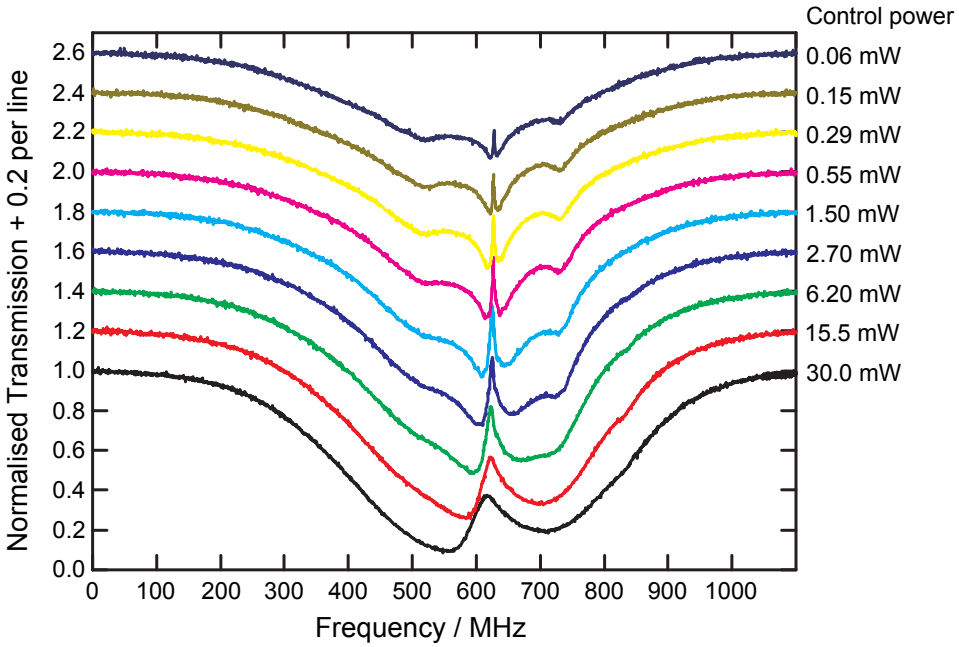

Figure 5.3 EIT peaks on the D_2 line in a standard cell for the hyperfine scheme, with linearly orthogonal polarisations of signal and control, cell is at 53°C, probe power of 37 μW for varying control powers. The EIT peaks become higher and broader for increasing control power but they also lie in a deeper valley caused by the additional pumping of the control laser. The additional features to the side of the EIT peaks, especially at lower control powers are velocity-selective optical pumping (VSOP) features.

temperature the Doppler profiles overlap. The result is optical pumping from the F=2 level into the F=1 level. This means that the probe beam sees more atoms in the F=1 state than the usual thermal distribution, and so the probe undergoes more absorption, increasing the depth of the absorption. In [75], explicit calculations of the effects of the additional energy levels on a Doppler broadened system are conducted with a density matrix formalism extended to cover all these levels. The absorption spectra calculated show the behaviour measured in Fig. 5.3. The additional features in the plot are due to velocity-selective optical pumping (VSOP). These features, when not familiar with them, can be easily confused with the laser not running in single mode. But some analysis confirms that the VSOP dips are exactly in the expected locations. This phenomenon is also investigated in [38]. The usual Doppler-free (counter-propagating) spectroscopy relies on VSOP. As long as there are additional levels within the Doppler broadened profile VSOP can be observed [37]. Here the two beams are co-propagating.

In order for optimal slow light effects EIT peaks with narrow spectral width are needed, giving steep linear dispersion for the slowest group velocity, and which rise to 100% so that the pulse is not absorbed. Given that these are not observed it can be concluded that the D_2 line is unlikely to provide a good candidate for a quantum memory.

5.2.3 Zeeman EIT on D_1 line

5.2.3.1 Standard cell

Investigations then moved to a simple Zeeman scheme on the D_1 line between the m_F states of the F=2 and F'=1 levels. The control and probe are given orthogonal circular polarisations, say σ_+ for the control and σ_- for the probe. The much higher strength of the control relative to the probe means that very quickly all the population ends up in the F=2, m_F=2 level, $|1\rangle$. The state $|2\rangle$ is the F=2, m_F=0 state and $|3\rangle$ is the F'=2, m_F=1 state. The control detuning was set to 160 MHz with one AOM, and the probe is scanned with a second AOM. The beam width ($w = 1/\mathrm{e}^2$) of the control beam was 0.60±0.02 mm.

The suppression of the control beam was not optimal. In particular, some of the control power acquired a horizontal rather than vertical polarisation, and thus was not removed by the Glan-Laser polarising beam cube. Approximately 1:4000 of the control power eventually made it through to the photodiode, with 7 μW of control power leaking if the control was 30 mW, which is of comparable magnitude to the probe power of 37 μW. To see what effect this will have, assume the two components have the same magnitude E field and let $\delta\omega(t)$ be a time varying shift in the frequency, then the resultant field will be

$$E\sin\omega t + E\sin(\omega + \delta\omega(t)t) = 2E\cos\left[\frac{(\delta\omega(t)t)}{2}\right]\sin\frac{(2\omega + \delta\omega)t}{2}.$$

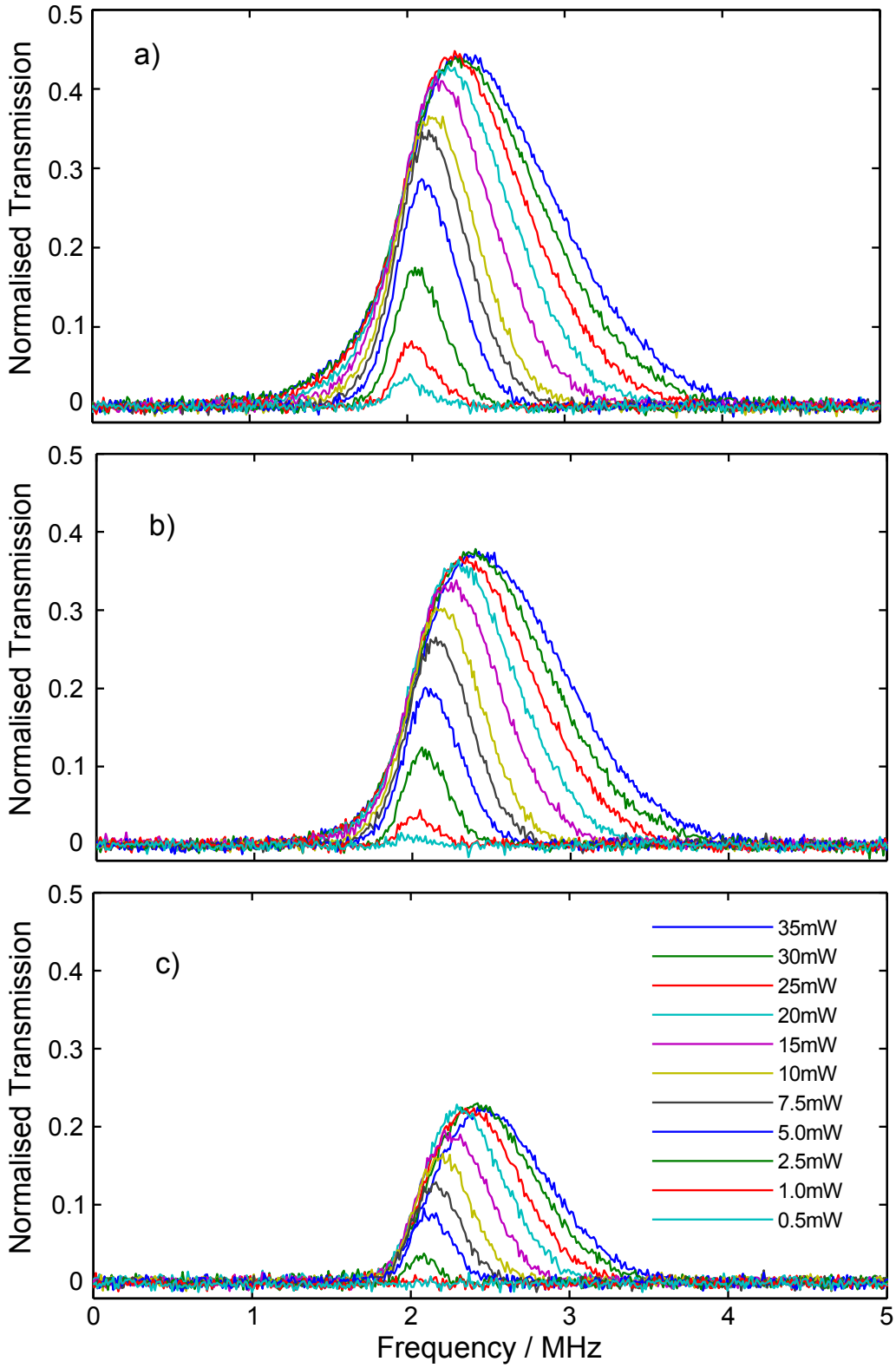

Figure 5.4 EIT peaks for a standard Rb cell at a) 74.2°C, b) 77.3°C and c) 82.9°C at varying control powers. The lines correspond to control powers, from top to bottom, of: 35, 30, 25, 20, 15, 10, 7.5, 5, 2.5, 1 and 0.5 mW. The traces from the photodiode have been directly send through an electronic low pass filter (1 MHz cut-off) to remove residual beat noise between leaking control and probe. A small magnetic field was applied deliberately so that probe and control would need a frequency difference of about 10 MHz to be on two-photon resonance in order to allow the low pass filtering.

The sine term oscillating at twice the light frequency is far too high frequency to be picked out directly by the photodiode, but the cosine term is within the bandwidth of the photodiode and the ramped frequency gives a chirped signal, of maximum intensity when the laser frequencies are equal.

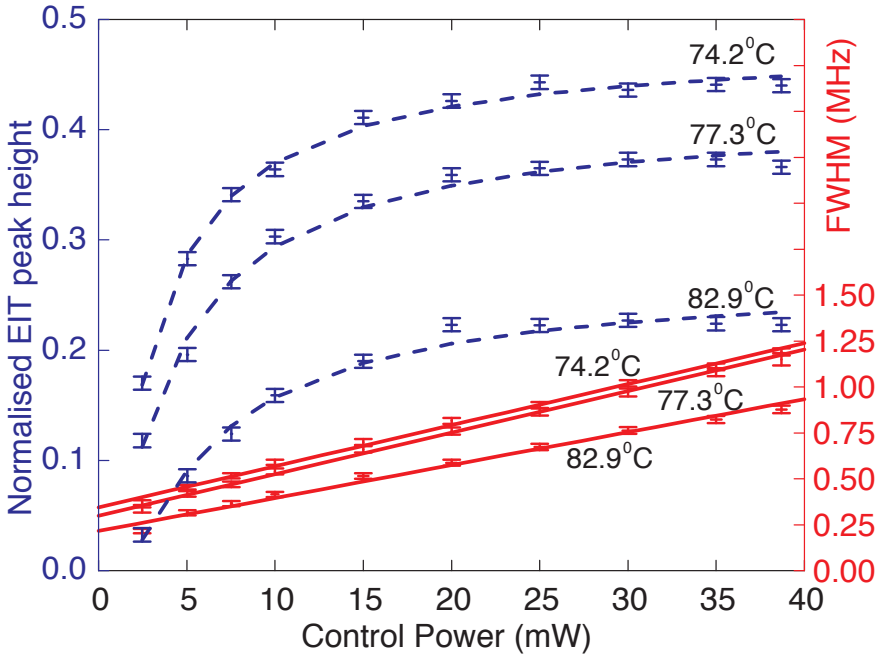

Figure 5.5 Full width at half maximum in red and normalised peak height of the EIT features in Fig. 5.4 as a function of control power. A linear fit has been applied to 5 mW and above for the FWHM, and the peak heights have been fitted as described in the text. Error bars calculated from uncertainty in locating the FWHM, temperature drifts and control intensity fluctuations.

The PBS on which the beams were combined was replaced by a second Glan-Laser, and it was ensured all the polarisation optics were optimally orientated. However, the suppression could not be further improved. Instead, a magnetic field was applied using a current of 2.15 A to give a measured Zeeman splitting of $\sim$10 MHz, lifting the degeneracy in the m_F states and moving the two photon resonance away from point where the probe and control frequencies are equal. The residual chirp between the two lasers was removed by an electronic low pass filter with a cut-off of 1 MHz.

The cell was heated to three different temperatures, 74.2°C, 77.3°C and 82.9°C corresponding to atomic densities of 2.6×10^{11} cm^{-3}, 3.4×10^{11} cm^{-3} and 6.8×10^{11} cm^{-3}. The EIT transmission features measured are shown in Fig. 5.4. With no control, the cell was opaque to the probe. As the power increased, so did the height and the width of the transmission window, to a maximum of 44% transmission at 74.2°C.

Fig. 5.5 shows the FWHM and peak heights of the EIT features as a function of the control power. A straight line has been fitted to FWHM data, with R^2 correlation coefficients ranging from 0.998 to 0.993 indicating a good linear fit. This confirms the dependence of the EIT width on the Rabi frequency from Eq. (2.11), since the control power P is related to the Rabi frequency by [35, 41]:

$$|\Omega_c|^2 = \left(\frac{1}{\hbar}\right)^2 \left(\frac{4P}{\pi c \varepsilon_0 w^2}\right) |\langle 1|e\vec{r}|3\rangle|^2 \quad , \tag{5.1}$$

where w is the beam waist. The linear dependence does not extend to powers below 2.5 mW (not shown in Fig. 5.5), but nor would one expect it to since the assumption that $\Omega_c \gg \Omega_p$ is no longer valid. From the positive y-intercept one can also conclude that $\gamma_{31}\gamma_{21}$ is non-zero (see (2.11)).

Also shown in Fig. 5.5 is the peak height of the features as a function of control. The expected fit taken from (2.10) and shown as a blue line in Fig. 5.5 is $y = A\exp(B/(C + D|\Omega_c|^2))$. This fit seems to overshoot the dataset for higher control powers, an unexpected behaviour possibly caused by Doppler broadening. In [31] it is suggested that a $\frac{1}{|\Omega_c|^4}$ dependence may be observed if the Rabi frequency is larger than the Doppler broadening. This is not the case for the results here, since largest powers used were 38 mW, corresponding to a Rabi frequency of 80 MHz compared to a Doppler broadening of ∼560 MHz at these temperatures, but it is possible that some intermediate regime may operate.

5.2.3.2 Buffered cell

Investigated was an EIT scheme between Zeeman substates on the F=2 and F'=1 levels of the D_1 line (see Fig. 5.2(a)) in cell 1, the ^{87}Rb and 10 Torr Ne cell. The control beam was given circular σ_+ polarisation, while the probe beam had orthogonal σ_- circular polarisation, achieved by placing a quarter-wave plate in front of the cell. By placing another quarter-wave plate after the cell, the control and probe were re-linearised to horizontal and vertical polarisations, respectively. Another half wave plate was present in order to make fine adjustments to the polarisations' orientations, compensating for inefficiencies in the quarter-wave plates, and birefringence of the cell windows.

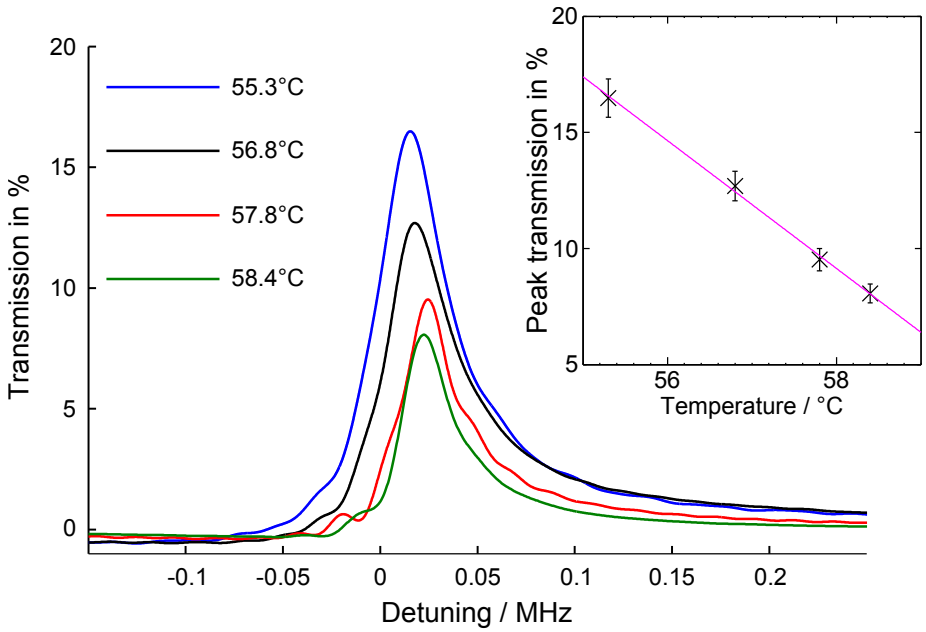

Figure 5.6 Close-up of the EIT feature for a few different temperatures, in the Zeeman scheme on the D_1 line. The peaks, from top to bottom, have FWHMs of 178, 178, 140, and 126 kHz, respectively.

Both beams originated from one laser. The control beam was tuned to the F=2$\rightarrow$ F'=1 transition, while the signal beam was modulated by the probe AOM to either pulse or scan, but with frequencies in the same vicinity as the control. The AOMs used here have a narrow operating range of a couple of ten MHz around their design frequency of 80 or 110 MHz for

which they provide maximum diffraction efficiency. This meant that the frequency difference between the two beams was limited to approximately $\pm$15 MHz.

Using the EIT setup (Fig. 5.1), the probe was scanned $\pm$2 MHz around the resonance, while keeping the control at constant intensity and frequency (Fig. 5.6).

5.2.4 Hyperfine-EIT on D_1 line

Investigations were continued using another EIT scheme, still on the D_1 line in cell 1, where the Λ-scheme groundstates lay on different hyperfine levels (see Fig. 5.2(d)). The second laser was now operational again, and was coupled into the control AOM and the control fibre-coupler, while the other laser remained as the probe, so that it was possible to vary the frequency of the two beams independently. The control beam was tuned to the F=2$\rightarrow$ F'=1 transition, and the probe beam had frequencies centred around the F=1$\rightarrow$ F'=1 transition. The new setup had the advantage that the probe could now be scanned over the entire D_1 line, a frequency range of about 8 GHz, and that much more power was now available for the control beam, with a peak power of 17.1 mW, for a 3.5 mm beam diameter, giving a maximum intensity of 1.777 mW/mm^2, equaling 100 times the saturation intensity (16.7 μW/mm^2) [73].

Removing the two quarter-wave plates used for the Zeeman scheme, the control and probe were now vertically and horizontally polarised, respectively. The half-wave plate after the cell now served to turn each polarisation by 90°, so that the probe would be reflected by a PBS, and the control transmitted. This was done to improve the filtering, because the PBSs turned out to be more efficient in suppressing reflected horizontally polarised light than transmitting vertically polarised light.

Much purer polarisations were able to be produced when using linear, rather than circular, polarisations. So, for practical purposes, it is beneficial to work in a scheme where the neces-

sary atomic transitions are accessed via linearly polarised light. With the control beam tuned to the F=2$\rightarrow F'$=1 transition, and the probe scanning across several GHz in the vicinity of the F=1$\rightarrow F'$=1 transition, a spike in transmission could be immediately observed at the location of the F=1$\rightarrow F'$=1 transition (see Fig. 5.8). Varying the control power, an increase in transmission of 99% was observed at the F=1$\rightarrow F'$=1 resonance (see Fig. 5.7). Some of the scans, zoomed into the EIT peaks, are plotted on the inset graph in Fig. 5.8. The large peak in transparency can be attributed to a small γ_{12} value – associated with the decoherence time of the dark-state superposition in the vapour – owed to the buffer gas keeping the rubidium atoms in the beam path for a greater duration. In Fig. 5.8, the full-width-half-maxima of these EIT peaks are all roughly 0.5 MHz. Unfortunately, soon after starting the two-laser investigation, the MOGLabs laser became unavailable, as it had to be sent back for servicing. This means it was not possible to take scans in higher resolution, with at least twice as many points to accurately fit and characterise a Gaussian.

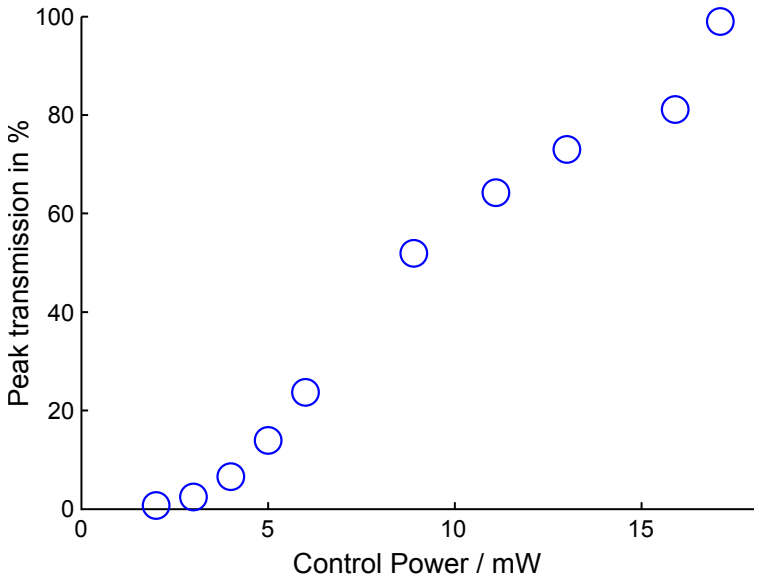

Figure 5.7 EIT peak height for different control powers, in the hyperfine scheme on the D_1 line in a standard cell.

Working on the Zeeman scheme, it was found that the pressure broadening caused by the buffer gas produced unwanted effects. However, by working in a similar scheme, using a static magnetic field to lift the energy degeneracy of the ground states, and utilising a lower pressure of buffer gas, results might prove useful. It would be worthwhile investigating EIT using the same setup, but with a wider range of cells with different buffer gas pressures, in order to find the optimum buffer gas pressure to ensure storage times of several pulse lengths while minimising detrimental effects like level-mixing through pressure broadening or collisional-induced fluorescence.

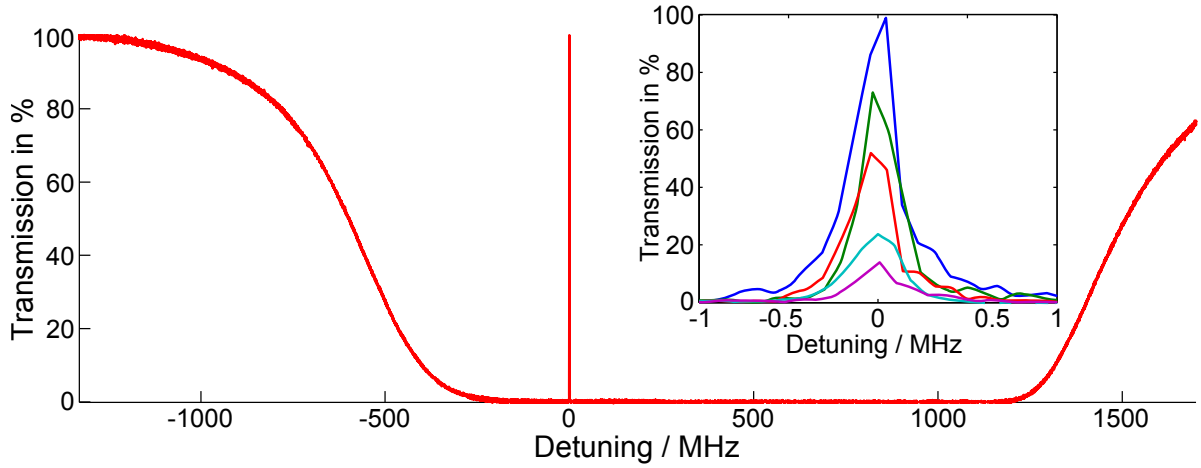

Figure 5.8 Weak-probe spectrum on D_1 line with control on F=2→F'=1, EIT peak visible for zero probe detuning from F=1→F'=1 resonance, for a control power of 17.1 mW. Inset: the same feature, with control powers of 17.1 mW, 13.0 mW, 8.9 mW, 6.0 mW, and 5.0 mW. Standard cell, no buffer gas, L =7.5 cm.

In Fig. 5.8 it can be seen that there are configurations where almost 100% EIT can be observed. In that particular measurement both lasers were free running.

Chapter 6

Slow light and stored light

Contents

6.1 Setup

The setup here is identical to the one used in EIT in the previous chapter.

6.2 Slow light and light storage results

6.2.1 Slow Light results

An operational temperature of ∼55°C was found to be the best to run 3.6 μs pulses through the cell (see Fig. 6.1). Other investigated pulses that were run through the cell had lengths of 10, 30 and 200 μs. Short delays, always roughly 10% of the pulse length, were observed. However, given that the 'delayed' pulses never move outside the envelope of the reference beam, and that the pulse delays do not display the expected $1/P$ dependence it is likely that the leading edge of the signal pulse was absorbed. Another alternative, is that the control beam power was too low, and that the strong control field approximation does not hold true here. The maximum output

from the control fibre-coupler was about 4 mW, compared to the 20 mW output from the laser, which has been diminished due to inefficiencies in the AOMs and fibre-coupling.

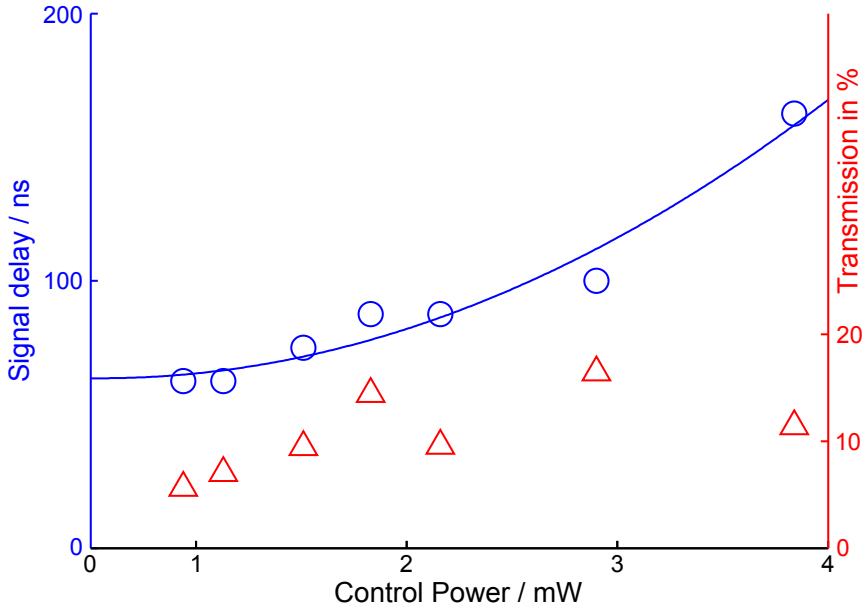

Figure 6.1 3.6 μs pulses propogating through cell 1 for different control powers, at temperatures of 55.5±0.5°C.

While the setup was still operational, a substantial pulse delay had been observed also. The delayed pulse was very noisy, at 2.2% of the height of the reference pulse, but it clearly lay outside the reference envelope, with a delay of 1.8 μs, for a control power of 4.77 mW (see Fig. 6.2).

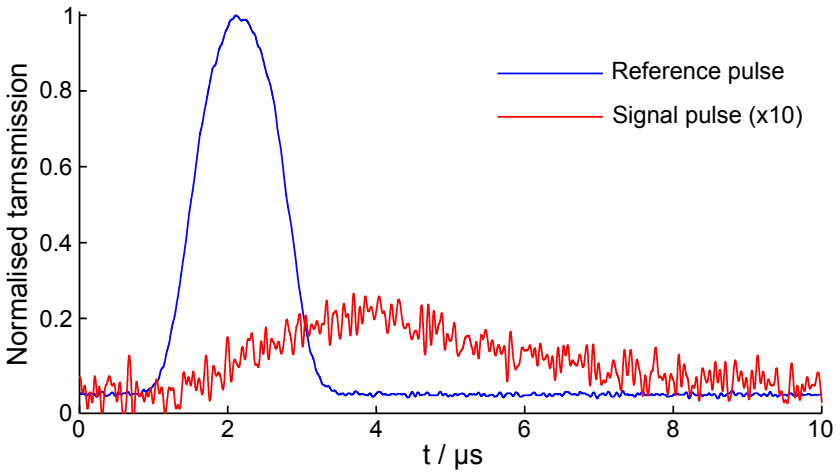

Figure 6.2 A 3.6 μs probe pulse delayed due to EIT, in the presence of a 4.77 mW control field. Horizontal axis is time in μs.

It was possible to observe slow light and pulse storage on the Zeeman scheme on the D_1 line. To take the results, no magnetic field was applied with the external solenoid, which allowed the μ-metal shield to be used. Both AOMs were set to the same driving frequency of 55 MHz, giving a detuning of 110 MHz double pass. At this point a separate problem connected with the leaking of probe light became apparent: the different beam paths taken by the probe and the control created a Mach-Zehnder interferometer. As vibrations or air circulations caused the different arms of the interferometer to change length, the phase between the probe and leaking control would change, and interference between them would vary. To minimise the noise as a percentage of the final signal, the probe power was increased to a peak of 300 μW, while ensuring that the medium was still opaque without the control.

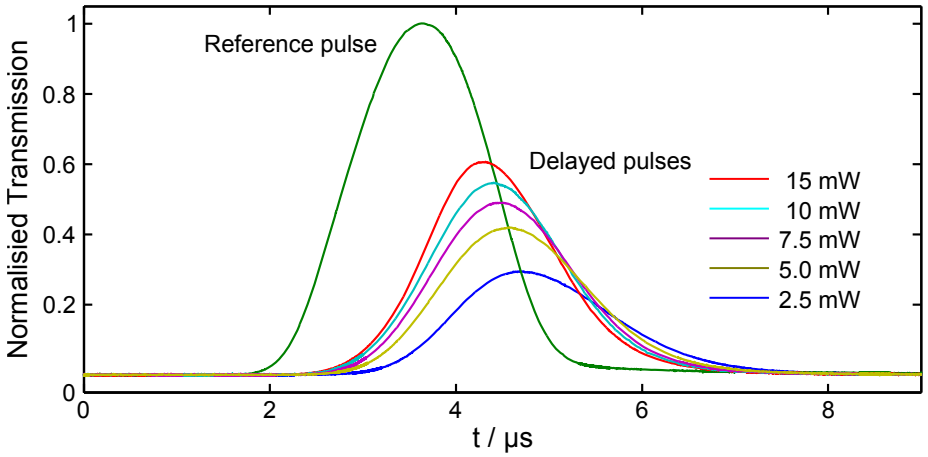

Figure 6.3 Slow light on Zeeman scheme, D_1 line, standard cell, T=74°C, L=75 mm. Delayed 3.4 μs pulse, for different control powers from top to bottom: 15, 10, 7.5, 5, 2.5 mW, averaged over 256 traces.

Pulse shaping of the probe was achieved by using the LeCroy arbitrary waveform generator to apply a cosine squared modulation to the RF signal driving the AOM. Data were taken for pulses of 6.9, 3.4, 1.8 and 0.77 μs duration. An identical reference pulse which did not pass through the cell, and had a height equal to the height of the probe beam with no absorption was used to measure the delay. A typical dataset is shown in Fig. 6.3 for a 3.4 μs pulse. The largest delay observed was for all pulse lengths at 2.5 mW, for a 10 μs pulse this gave 1.10 $\pm$ 0.02 μs

delay, corresponding to $v_g \approx \frac{c}{2.3 \cdot 10^4}$. As this was the lowest power setting tried for all pulses, it is likely that the higher delays would be observed for even lower powers, as predicted by (2.13). Also, the shorter pulses were attenuated more strongly than the longer pulses because their width in frequency space was too broad to fit under the EIT peak.

6.2.2 Storage results

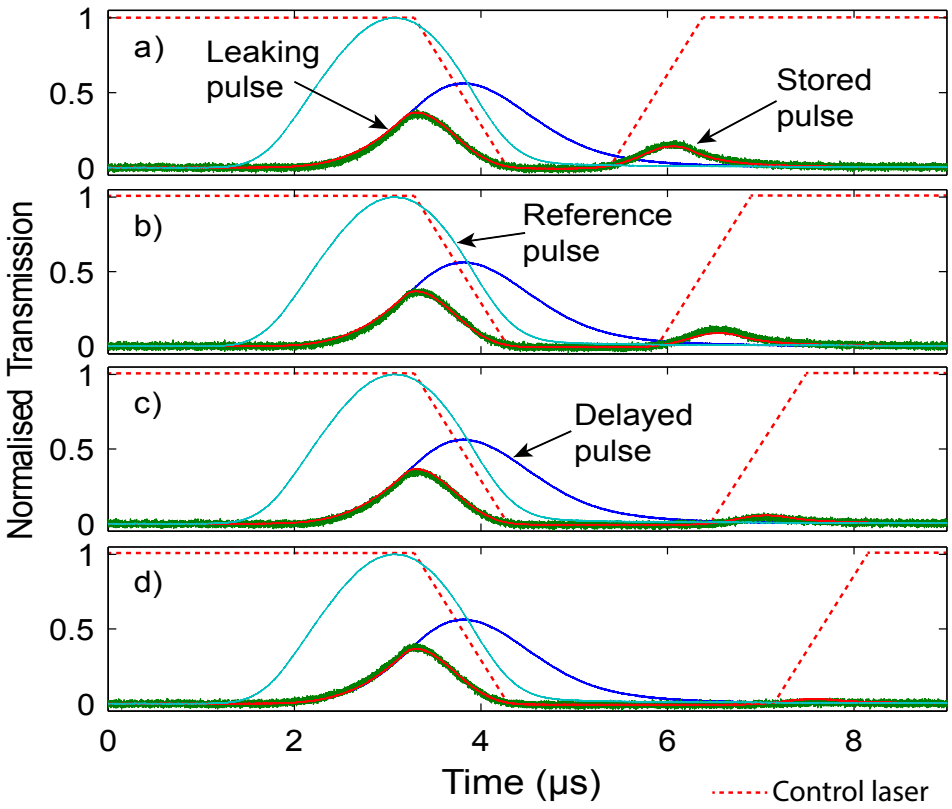

Figure 6.4 Pulse storage of a 3.4 μs pulse for a) 2.2 μs b) 2.7 μs c) 3.2 μs d) 3.7 μs in shown in green. For comparison, the averaged reference pulse (light blue), the delayed pulse (dark blue) and an averaged stored pulse (red) are also shown. The delayed pulse is shown to prove that the second peak is genuinely stored rather than just slow light. The storage times are calculated from the peak of the delayed pulse to the peak of the stored pulse.

Storage was achieved by turning down the control power to zero over 1 μs using an AOM while the peak of the pulse was in the medium. The stored pulse could be recovered after a variable time by ramping the control power back up over 1 μs. Finding optimal settings for storage of light in this scheme involves balancing a number of factors. Higher powers give

a higher and broader EIT peak, but lead to a faster group velocity. This in turn gives less pulse compression, to the point where the pulse does not fit inside the medium. Reducing the pulse length to compensate for this leads to further absorption because shorter pulses have a larger spectral width, as described above. It was found the shortest pulse which gives enough transmission through the medium for storage is a 3.4 μs pulse. With the least control power (2.5 mW) and slowest group velocity, this gives a compressed pulse length of 23 cm, more than three times the length of the cell. However, at 2.5 mW the stored pulse is too small to be readily distinguished from the background noise, so a higher power must be used.

The results shown in Fig. 6.4 were found with a 3.4 μs pulse and 10 mW of control power. This yields $v_{\mathrm{g}} = 125$ km/s and a compressed pulse of 43 cm in length. Although this is too long to fit in the cell, the central portion of the pulse could still be stored. The front part of the pulse which is not stored can be seen leaking through the cell in Fig. 6.4 as the first peak in the green trace.

A crude measure of the efficiency of the storage can be found by measuring the normalised peak height of a stored pulse. A 100% efficient memory would yield exactly the same height as the initial pulse. This measure neglects the fact that in the considered case here the front section of the pulse is not stored. The efficiency decreased rapidly as the storage time increased, ranging from 14% for 2.2 μs storage, to 3% for 3.7 μs storage. The stored pulse became indistinguishable from the background noise after longer storage times. This limited storage time is almost certainly caused by atoms leaving the beam path during the storage time, and working with a buffer gas cell with a suitable (not too high) buffer gas pressure will allow for longer storage times to be realised [25].

Both buffer gas cells with 40 Torr and 10 Torr of neon did not yield recognisable slow light and storage results. Their buffer gas pressure is therefore still deemed too high.

Chapter 7

Control Light Filtering Methods

Contents

In thermal ensembles it is necessary to have control and signal field co-propagating. For single photon storage and readout it is therefore important to filter out all the control light accidentally leaking into the signal mode since no control photon should be accidentally registered as a signal photon. This chapter lists the possible filtering methods and discusses their theoretical maximum attenuation figure of merit compared with experimentally achievable figures and discusses a feasible concatenation of filtering methods that should lead to a sufficient attenuation of the control field.

7.1 Polarisation filtering

Probably the easiest way of filtering control and probe beam is polarisation filtering, if the level scheme allows for applying fields of orthogonal polarisation. Worth mentioning that some schemes used by Novikova group use the same circular polarisation for signal and control in a hyperfine scheme. In this case polarisation filtering cannot be applied. Commercial polarising beam cubes (PBCs) specify attenuations of 10^{-2} to 10^{-8}. Experimentally I found that an

affordable standard PBC specified for 10^{-2}=20 dB attenuation could give up to 42 dB attenuation for p-polarisation found in the s-polarisation output port when the incidence angle was tuned slightly away (1-2 degrees) from normal incidence as depicted in Fig. 7.1. A much more expensive Glan-Laser polariser that was supposed to filter up to 50 dB in forward direction for one of the polarisations never lived up to its expectation. This polariser was found to perform just equal to the standard one under optimised angle. A possible explanation would be that a certain amount of light gets scattered at either one of the interfaces (entrance or exit facet or at the cemented section between the two wedges of the PBC) and that the scattered light has equal contributions of either polarisation.

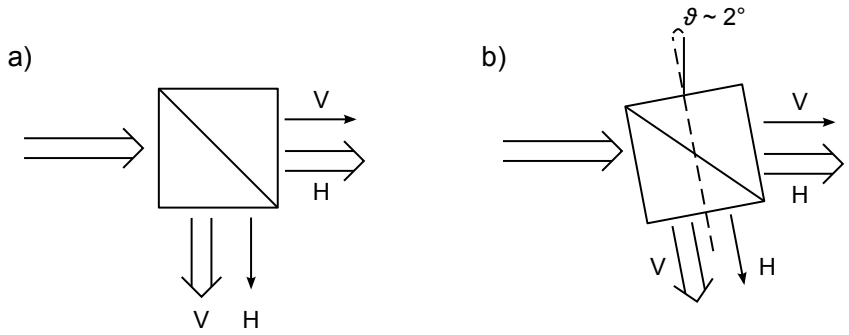

Figure 7.1 Different arrangements of a polarising beam cube (PBC). a) The laser beam is oriented to the entrance facet of the PBC under normal incidence. With this alignment the manufacturer's specification of 20 dB were always met. b) Rotating the PBC slightly away from normal incidence often holds a surprise. The residual fraction of p-polarised light (H) in the vertical output can be considerably smaller than in the case of normal incidence. In one case the rejection was as high as 42 dB.

7.2 Spatial filtering

Here two different ways of spatial filtering can be considered: a) Mode mismatch into an optical fibre. b) Introducing an angle between control and probe field.

The first method can be achieved by choosing a larger beam diameter for the control field. A fibre coupling stage is then arranged so that the much smaller probe field is maximally coupled which leads to the control beam poorly coupled. Since usually the probe field would be coupled

for subsequent detection anyway and choosing the control field leads to a more homogeneous control field intensity in the region of the probe field this method seems beneficial as long as the required control intensity can be guaranteed. Using this method (a) in Fig. 7.2) a suppression of 10^{-3} or 30 dB was achieved.

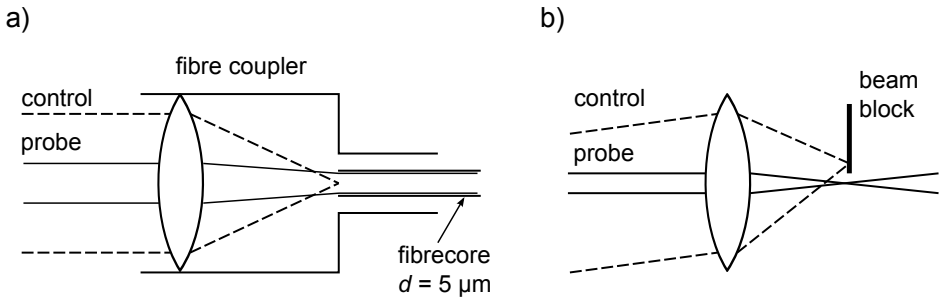

Figure 7.2 Two methods for spatial filtering. a) The probe beam is mode-matched to a single-mode fibre by means of a fibre coupler. The collinear but much larger control beam is focussed in the fibre coupler to a much smaller focus size and therefore mismatched with the accepting mode of the fibre core. b) The control is angled with respect to the probe beam and are sent through a lens. Due to the angle the focus of the control beam will be off-axis and can be separated with a knife-edge or beam block.

The second method would be angular mismatch or deviation. The disadvantage here is that the EIT efficiency decreases rapidly with increasing angle. Angles on the order of less than 1 mrad essentially deteriorate the EIT signal significantly (c.f. Fig. 2 in [64]). But the authors claim that the expected broadening at a given angle should be much higher (three orders of magnitude) than what they measured, and they attribute this to the buffer gas inducing a "Dicke-type narrowing" that heavily mitigates the effect of angular detuning. Dicke narrowing refers to the effect predicted in [76] that occurs when an emitter or absorber is confined to a volume with dimensions on the order of the transition wavelength.[1] Although in the context of EIT in buffered vapour cells this explanation has also been criticized by Iftiquar [77].

It is not clear how the findings in [64] with respect to the angling of probe and control are applicable to this thesis since they investigated EIT resonances ∼10 kHz in width, 2 orders of

[1]The derivation in [76] is done in 1D. In 3D the relevant magnitude would be the mean free path which for Rb buffered by Ne starts to get in the range of the D_1 transition wavelength for buffer gas pressures of 40 Torr and higher.

magnitude smaller than targeted in this thesis. Also they only specify "arbitrary units" for the transmission which is not useful for a comparison.

So far no experiment has mapped out the effect of angle detuning varying angle *and* varying the buffer gas pressure to come to a definite conclusion how much Dicke narrowing contributes.

7.3 Rb filter cell (85/87)

Vapour cell filtering (as implemented in [29]) is where the combined beam output from an experimental cell is directed through another cell, the contents of which have a large optical depth in the vicinity of the control beam's frequency, but negligible absorption at the probe frequency, e.g. achievable by using a nitrogen (N_2) buffered ^{85}Rb cell. Figure 7.3 quantitively shows how well such a setup could work.

For the purpose of filtering the control beam in a hyperfine scheme a ^{85}Rb cell with 120 Torr of nitrogen was ordered. The idea here is to shift the ^{85}Rb resonance by such an amount that the ^{85}Rb F=3 manifold lines up with the ^{87}Rb F=2 manifold. Using the standard alkali reference Steck Data one can work out that a shift of approx. 1.3 GHz is required in this case.

The work of Rotondaro [48] helped identifying that methane, nitrogen and argon (amongst the gases that were investigated in their work) provide the largest line shifts of -7.92, -7.41, -6.77 MHz/Torr, respectively. But since the broadening coefficients for these three gases are 29.1, 16.3 and 18.1 MHz/Torr, respectively, and broadening was to be minimised, nitrogen provided the smallest additional broadening. Therefore nitrogen was chosen.

That such filtering is possible is well known since before the invention of the laser. The most prominent application that uses different rubidium isotopes for light frequency filtering the Rb optical clock.

In the field of single photon storage one of the first to make use of a filter cell is the ex-

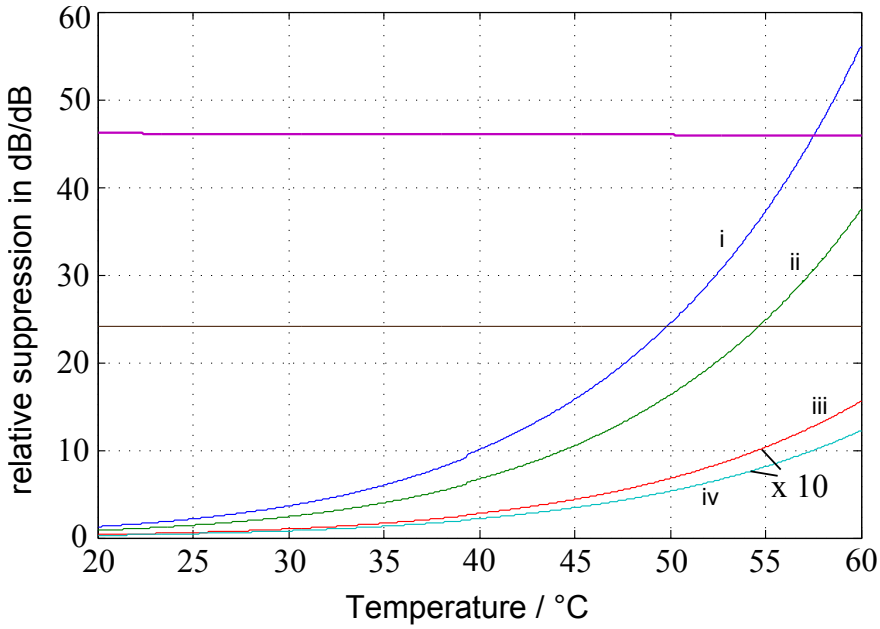

Figure 7.3 Ability of a ^{85}Rb filter cell (of 150 mm length and filled with 120 Torr of nitrogen as buffer gas) to suppress the control field whilst maintaining acceptable transmission for a signal field. It is assumed here that the ^{85}Rb vapour has been fully pumped into the F=3 ground state (^{85}Rb has a nuclear spin of 5/2 [47]). The curve i(ii) is the control field tuned to the F=2$\leftrightarrow F'$=1(2) resonance, while curve iii(iv) is the probe field near the F=1$\leftrightarrow F'$=1(2) resonance. The purple trace is the suppression of the control field divided by the suppression of the signal field, both addressing the F'=2 in ^{87}Rb which is essentially constant (46 dB/dB) with temperature. The other horizontal trace is for addressing the F'=1 state (24 dB/dB). This means, for example, that a 100,000 fold suppression of the control could be achieved at only 1dB loss (80% transmission) of the probe signal with the 120 Torr ^{85}Rb cell.

periment at Harvard from Eisaman et al. This is also reported in their highly-cited Nature publication [29]. [2]

Since at the time of ordering the filter cell it was not clear if an EIT scheme in ^{87}Rb would eventually connect via the excited state F'=1 or F'=2 a nitrogen pressure was chosen so that the center of the ^{85}Rb F=3 resonance was shifted in between the ^{87}Rb F=2$\rightarrow F'$=1 and F=2$\rightarrow F'$=2 lines. This obviously does not maximise the filtering for either of the lines but promised to give more flexibility. The shift for the D_1 line is -7.41 ± 0.12 MHz/Torr [48]. Therefore to produce the necessary shift a pressure of 120 Torr was required. (The shifts due to neon in the ^{87}Rb cells were neglected here as they only amount to tens of MHz.) Unfortunately 120 Torr of nitrogen also leads to considerable collisional broadening on the order of $\sim$2 GHz.

With the model developed it is possible to calculate the theoretical ability to suppress the control beam whilst providing high transmission for the signal field. This is displayed in Fig. 7.3 for the ^{85}Rb cell. Interestingly, dividing the two attenuations (in dB) leads to a constant. This means, if an acceptable probe attenuation value can be specified this "attenuation per attenuation" value can be used to calculate the achievable control attenuation.

Using the model should enable one to find an even better value for the buffer gas pressure if the transition that one wants to run EIT on is known.

Here control photons are absorbed and re-emitted into a 4π solid angle. This still bears the risk of re-emission into the forward direction. Therefore this filtering stage should be used behind other filtering methods since spontaneously re-emitted photons will acquire their polarisation at random.

It is yet to be shown which permutation of filtering methods would provide the best overall attenuation.

[2] Unfortunately, none of the parameters regarding the ^{85}Rb filter cell (temperature, length, isotope purity, buffer gas and buffer gas pressure) are explained (not even in Eisaman's thesis).

7.4 Etalon / Fabry Perot

An etalon would be a good way of filtering. The approach here is to choose the free spectral range twice as large as the frequency difference of control and signal so that the signal would hit the etalon resonance and the control would be exactly off-resonant to provide maximum rejection. The etalon line width should then be chosen so that the signal suffers the least amount of rejection. This choice then fully determines the required finesse and the reflectivities of the two mirrors or facets in case of a solid etalon. Purchasing a custom-made etalon has been abstained from due to budget limits and could therefore not be further investigated.

Chapter 8

Conclusions & Outlook

Contents

Summed up, this work attempted to investigate the compatibility of a CQED-based single photon source and an EIT-based memory in its particular realisation of a single ^{87}Rb atom in a high-finesse cavity and ^{87}Rb vapour in a glass cell with added buffer gas.

Having investigated EIT on two different schemes in ^{87}Rb vapour in a 10 Torr neon buffer and in an unbuffered cell, this work indicates that the hyperfine scheme on the D_1 absorption line will be a good candidate for light storage, given the high transparency ($\sim$99%), the potentially large compression of a signal pulse in the cell, and the degree of precision with which we can control the polarisation of the control and probe beams.

8.1 Conclusion

Over the course of this project EIT and associated phenomena have been observed on both the D_1 and D_2 lines. While the D_2 line has practical advantages vis a vis the single photon source, it was found not to be suitable for an efficient quantum memory system because a high proportion of the pulse light is absorbed. This can be attributed to the close spacing of the excited $5p\ ^2P_{3/2}$ manifold within the Doppler width [78]. Optical pumping may ameliorate the

situation, as shown in Fig. 5.3 and as argued by [38], but it seems that a high contrast EIT peak with corresponding steeply sloped dispersion necessary for slow light and storage cannot be achieved.

On the other hand, it was found that the D_1 line can be used to store weak light pulses. The storage times here are on the order of a few μs as expected without buffer gas, since this is the approximate time taken for atoms to traverse the beam (4 μs). Longer storage times will be achieved by the use of a vapour cell with a buffer gas (typically neon) at a pressure of between 7 and 40 Torr. This effectively removes the population exchange between atoms inside and outside of the beam by reducing the mean free path of the rubidium atoms, confining them to the beam during the timescale over which the memory would be active. Paraffin coating could reduce the dephasing collisions with the walls, and further layers of magnetic shielding can also be used to block stray magnetic fields. Lower decoherence rates would allow lower control powers, giving slower light, and larger optical depths, both of which eventually could lead to complete localisation of the pulse within the medium.

The interferometric effects can be removed either by implementing a phase lock between the two beams, or by moving to spatial rather than polarisation filtering. The two beams could be crossed, overlapping in the cell but sufficiently misaligned at the photodiode to allow the control to be blocked. Better filtering would also allow weaker probe powers to be used, as these signals would not be masked by leaking control power. Alternatively, a hyperfine Λ-scheme on the D_1 line could be implemented.

The progress in this project clearly indicates that straightforward refinements to the scheme should enable pulse storage over longer timescales and greater efficiencies, and ultimately progress to a single photon quantum memory.

8.2 Outlook

By including additional beam filtering methods, such as vapour-cell filtering, and spatial filtering, the setup we have used could, in the future, be used for storage of single photons, once a 10^{12} suppression of the control beam can be achieved. So far, we only filter using polarising beam splitters, which suppresses the control beam by a factor of 10^4.

References

[1] E Knill, R Laflamme, and Gerard J. Milburn. A scheme for efficient quantum computation with linear optics. *Nature*, 409(6816):46–52, January 2001. 1.1

[2] Christopher Monroe. Quantum information processing with atoms and photons. *Nature*, 416(6877):238–46, March 2002. 1.1

[3] H. Jeff Kimble. The quantum internet. *Nature*, 453(7198):1023–30, June 2008. 1.1

[4] Lene Vestergaard Hau, Stephen E. Harris, Zachary Dutton, and Cyrus H Behroozi. Light speed reduction to 17 metres per second in an ultracold atomic gas. *Nature*, 397(February):594–598, 1999. 1.3

[5] Michael Fleischhauer, Susanne F. Yelin, and Mikhail D. Lukin. How to trap photons? Storing single-photon quantum states in collective atomic excitations 1. *Optics Communications*, (May):395–410, 2000. 1.3

[6] Irina Novikova, Nathaniel B. Phillips, and Alexey V. Gorshkov. Optimal light storage with full pulse-shape control. *Physical Review A*, 78(2):1–4, August 2008. 1.3, 3.3

[7] Irina Novikova, David F. Phillips, and Ronald L. Walsworth. Slow Light with Integrated Gain and Large Pulse Delay. *Physical Review Letters*, 99(17):1–4, October 2007. 1.3

[8] Michael Fleischhauer and Mikhail D. Lukin. Quantum memory for photons: Dark-state polaritons. *Physical Review*, 65, 2002. 1.3

[9] Nathaniel B. Phillips, Alexey V. Gorshkov, and Irina Novikova. Optimal light storage in atomic vapor. *Physical Review A*, 78(2):1–9, August 2008. 1.3, 3.3

[10] Alexey V. Gorshkov, Axel André, Michael Fleischhauer, Anders S. Sø rensen, and Mikhail D. Lukin. Universal Approach to Optimal Photon Storage in Atomic Media. *Physical Review Letters*, 98(12):123601, 2007. 1.3

[11] Alexey Gorshkov, Axel André, Mikhail Lukin, and Anders Sorensen. Photon storage in Λ-type optically dense atomic media. II. Free-space model. *Physical Review A*, 76(3):033805, September 2007. 1.3, 2.2.2

[12] J Kim, Oliver Benson, H. Kan, and Yoshihisa Yamamoto. A single-photon turnstile device. *Nature*, 397(6719):500–503, 1999. 1.4

[13] Christian Kurtsiefer, Sonja Mayer, Patrick Zarda, and Harald Weinfurter. Stable Solid-State Source of Single Photons. *Physical Review Letters*, 85(2):10–13, 2000. 1.4

[14] Rosa Brouri, Alexios Beveratos, Jean-philippe Poizat, and Philippe Grangier. Photon antibunching in the fluorescence of individual color centers in diamond. *Optics Letters*, 25(17):1294–1296, 2000. 1.4

[15] P. Michler, Atac Imamoglu, Md Mason, Pj Carson, Gf Strouse, and Sk Buratto. Quantum correlation among photons from a single quantum dot at room temperature. *Nature*, 406(6799):968–70, August 2000. 1.4

[16] Charles Santori, Matthew Pelton, Glenn S. Solomon, Yseulte Dale, and Yoshihisa Yamamoto. Triggered Single Photons from a Quantum Dot. *Physical Review Letters*, 86(8):1502–1505, 2001. 1.4

[17] Z. Yuan, B.E. Kardynal, R Mark Stevenson, A.J. Shields, C.J. Lobo, K. Cooper, N.S. Beattie, D.A. Ritchie, and M. Pepper. Electrically Driven Single-Photon Source. *Science*, 295(5552):102, 2002. 1.4

[18] E. Moreau, I. Robert, J. M. Gerard, I. Abram, L. Manin, and V. Thierry-Mieg. Single-mode solid-state single photon source based on isolated quantum dots in pillar microcavities. *Applied Physics Letters*, 79(18):2865, 2001. 1.4

[19] B Lounis and W E Moerner. Single photons on demand from a single molecule at room temperature. *Nature*, 407(6803):491–3, September 2000. 1.4

[20] Juan I. Cirac, Peter Zoller, H. Jeff Kimble, and Hideo Mabuchi. Quantum state transfer and entanglement distribution among distant nodes in a quantum network. *Physical Review Letters*, 78:3221–3224, 1997. 1.4

[21] Alexander I. Lvovsky, Barry C. Sanders, and Wolfgang Tittel. Optical quantum memory. *Nature Photonics*, 3(12):706–714, December 2009. 1.4

[22] A.R. Dixon, Z.L. Yuan, J.F. Dynes, A.W. Sharpe, and A.J. Shields. Continuous operation of high bit rate quantum key distribution. *Applied Physics Letters*, 96(16), 2010. 1.4

[23] H J Briegel, W Dür, J I Cirac, and P Zoller. Quantum repeaters: The role of imperfect local operations in quantum communication. *Physical Review Letters*, 81(26):5932–5935, 1998. 1.4

[24] L. M. Duan, M. D. Lukin, J. I. Cirac, and P. Zoller. Long-distance quantum communication with atomic ensembles and linear optics. *Nature*, 414(6862):413–418, November 2001. 1.4

[25] D. F. Phillips, A. Fleischhauer, A. Mair, R. L. Walsworth, and M. D. Lukin. Storage of light in atomic vapor. *Phys. Rev. Lett.*, 86(5):783–786, Jan 2001. 1.4, 2.2.2, 6.2.2

[26] Chien Liu, Zachary Dutton, Cyrus H. Behroozi, and Lene V. Hau. Observation of coherent optical information storage in an atomic medium using halted light pulses. *Nature*, 409(6819):490–493, January 2001. 1.4

[27] J. J. Longdell, E. Fraval, M. J. Sellars, and N. B. Manson. Stopped Light with Storage Times Greater than One Second Using Electromagnetically Induced Transparency in a Solid. *Physical Review Letters*, 95(6), August 2005. 1.4

[28] T. Chanelière, D. N. Matsukevich, S. D. Jenkins, S. Y. Lan, T. A. B. Kennedy, and A. Kuzmich. Storage and retrieval of single photons transmitted between remote quantum

memories. *Nature*, 438(7069):833–836, December 2005. 1.4

[29] Matthew D. Eisaman, Axel André, F. Massou, Michael Fleischhauer, Alexander S. Zibrov, and Mikhail D. Lukin. Electromagnetically induced transparency with tunable single-photon pulses. *Nature*, 438(7069):837–41, December 2005. 1.4, 7.3, 7.3

[30] S. E. Harris, J. E. Field, and A. Imamoğlu. Nonlinear optical processes using electromagnetically induced transparency. *Phys. Rev. Lett.*, 64(10):1107–1110, Mar 1990. 2.2.1

[31] Michael Fleischhauer, Atac Imamoglu, and Jonathan P. Marangos. Electromagnetically induced transparency: Optics in coherent media. *Reviews of Modern Physics*, 77(2):633–673, July 2005. 2.2.1, 2.2.1, 2.2.1, 2.2.1, 2.2.2, 5.2.3.1

[32] Xian-min Jin, Jian Yang, Han Zhang, Han-ning Dai, and Sheng-jun Yang. Quantum interface between frequency-uncorrelated down-converted entanglement and atomic-ensemble quantum memory. *Science And Technology*, pages 1–28. 2.2.1, 2.2.1

[33] Graham T Purves. *Absorption & Dispersion in Atomic Vapours: Applications to Magnetometry*. PhD thesis, Durham University, 2006. 2.2.1

[34] Claude Cohen-Tannoudji, Jacques Dupont-Roc, and Gilbert Grynberg. *Atom-Photon Interactions: Basic Processes and Applications*. Wiley-Interscience, March 1992. 2.2.1

[35] C. J. Foot. *Atomic Physics (Oxford Master Series in Atomic, Optical and Laser Physics)*. Oxford University Press, February 2005. 2.2.1, 3.3.1.1, 4.1, 4.2.2, 5.2.3.1

[36] M. D. Lukin, M. Fleischhauer, A. S. Zibrov, H. G. Robinson, V. L. Velichansky, L. Hollberg, and M. O. Scully. Spectroscopy in dense coherent media: Line narrowing and interference effects. *Phys. Rev. Lett.*, 79(16):2959–2962, Oct 1997. 3

[37] Shrabana Chakrabarti, Amitkiran Pradhan, Biswajit Ray, and Pradip N Ghosh. Velocity selective optical pumping effects and electromagnetically induced transparency for D 2 transitions in rubidium. *Journal of Physics B: Atomic, Molecular and Optical Physics*, 38(23):4321–4327, December 2005. 2.2.1, 5.2.2

[38] O. S. Mishina, M. Scherman, P. Lombardi, J. Ortalo, D. Felinto, a. S. Sheremet, A. Bramati, D. V. Kupriyanov, J. Laurat, and E. Giacobino. Electromagnetically induced transparency in an inhomogeneously broadened Λ transition with multiple excited levels. *Physical Review A*, 83(5):053809, May 2011. 2.2.1, 5.2.2, 8.1

[39] Lene V. Hau, S. E. Harris, Zachary Dutton, and Cyrus H. Behroozi. Light speed reduction to 17 metres per second in an ultracold atomic gas. *Nature*, 397(6720):594–598, February 1999. 2.2.2

[40] D. Budker, D. F. Kimball, S. M. Rochester, and V. V. Yashchuk. Nonlinear Magnetooptics and Reduced Group Velocity of Light in Atomic Vapor with Slow Ground State Relaxation. *Physical Review Letters*, 83(9):1767–1770, August 1999. 2.2.2

[41] R. Paschotta. Encyclopedia of laser physics and technology. available online at http://www.rp-photonics.com/. 2.2.2, 5.2.3.1

[42] Irina Novikova, David F. Phillips, and Ronald L. Walsworth. Slow light with integrated gain and large pulse delay. *Phys. Rev. Lett.*, 99(17):173604, Oct 2007. 2.2.2

[43] Alexey V. Gorshkov, Axel André, Michael Fleischhauer, Anders S. Sørensen, and Mikhail D. Lukin. Universal approach to optimal photon storage in atomic media. *Phys. Rev. Lett.*, 98(12):123601, Mar 2007. 2.2.2

[44] Alexey Gorshkov, Axel André, Mikhail Lukin, and Anders Sorensen. Photon storage in Λ-type optically dense atomic media. I. Cavity model. *Physical Review A*, 76(3):033804, September 2007. 2.2.2

[45] Alexey Gorshkov, Axel André, Mikhail Lukin, and Anders Sorensen. Photon storage in Λ-type optically dense atomic media. III. Effects of inhomogeneous broadening. *Physical Review A*, 76(3):033806, September 2007. 2.2.2

[46] Paul Siddons, Nia C Bell, Yifei Cai, Charles S. Adams, and Ifan G Hughes. A gigahertz-bandwidth atomic probe based on the slow-light Faraday effect. 3(April):225–229, 2009. 2.3

[47] Daniel Adam Steck. Rubidium 85 D Line Data Author contact information :. 3.1.1, 2, 7.3

[48] Matthew D. Rotondaro and Glen P. Perram. Collisional Broadening and Shift of the Rubidium D_1 and D_2 lines ($5^2S_{1/2} \rightarrow 5^2P_{1/2}, 5^2P_{3/2}$) by rare gases, H_2, D_2, N_2, CH_4 and CF_4. *Journal of Quantitative Spectroscopy and Radiative Transfer*, 57(4):497–507, 1997. 3.1.1, 4.2.2, 7.3, 7.3

[49] J. Tidstrom. *Slow and stopped light by light-matter coherence control*. PhD thesis, KTH School of Information and Communication Theory, 2009. 3.1.2

[50] E A Donley, T P Heavner, F Levi, M O Tataw, and S R Jefferts. Double-pass acousto-optic modulator system. *Review of Scientific Instruments*, 76(6):063112, 2005. 3.1.4

[51] D. J. McCarron. A guide to acousto-optic modulators. Available online at massey.dur.ac.uk/resources/slcornish/AOMGuide.pdf, dec 2007. accessed on 10 April 2011. 3.1.4

[52] D. Phillips, Anett Fleischhauer, A. Mair, R. Walsworth, and M. Lukin. Storage of Light in Atomic Vapor. *Physical Review Letters*, 86(5):783–786, January 2001. 1, **??**, 3.3

[53] Irina Novikova, Alexey V. Gorshkov, David F. Phillips, Yanhong Xiao, Mason Klein, and Ronald L. Walsworth. Optimization of slow and stored light in atomic vapor. *Proceedings of SPIE*, 6482:64820M–64820M–11, 2007. 3.3

[54] C. J. Myatt, N. R. Newbury, and C. E. Wieman. Simplified atom trap by using direct microwave modulation of a diode laser. *Optics Letters*, 18(8):649, April 1993. 3.3, 3.3.1

[55] Irina Novikova. Optimizing stored light efficiency in vapor cells. *Proceedings of SPIE*, 5735:87–97, 2005. 3.3

[56] Irina Novikova, Yanhong Xiao, David F. Phillips, and Ronald L. Walsworth. EIT and diffusion of atomic coherence. *Journal of Modern Optics*, 52(16):2381–2390, 2005. 3.3

[57] Olivier Pinel, Mahdi Hosseini, Ben M Sparkes, Jesse L Everett, Daniel Higginbottom, Geoff T Campbell, Ping Koy Lam, and Ben C Buchler. Gradient echo quantum memory in warm atomic vapor. *Journal of visualized experiments : JoVE*, 1(81):e50552, January 2013. 3.3

[58] J E Bateman, R L D Murray, M Himsworth, H Ohadi, a. Xuereb, and T Freegarde. Hänsch–Couillaud locking of Mach–Zehnder interferometer for carrier removal from a phase-modulated optical spectrum. *Journal of the Optical Society of America B*, 27(8):1530, July 2010. 3.3

[59] Richard P Abel, Ulrich Krohn, Paul Siddons, Ifan G Hughes, and Charles S Adams. Faraday dichroic beam splitter for Raman light using an isotopically pure alkali-metal-vapor cell. *Optics letters*, 34(20):3071–3, October 2009. 3.3

[60] B E Unks, N A Proite, and D D Yavuz. Generation of high-power laser light with Gigahertz splitting. *Review of Scientific Instruments*, 78(8):083108, August 2007. 3.3, 3.4

[61] S. C. Bell, D. M. Heywood, J. D. White, J. D. Close, and R. E. Scholten. Laser frequency offset locking using electromagnetically induced transparency. *Applied Physics Letters*, 90(17):171120, 2007. 3.3, 3.3.1

[62] David Smith and Ifan Hughes. The role of hyperfine pumping in multilevel systems exhibiting saturated absorption. *American Journal of Physics*, 72(5):631, 2004. 3.3.1.1

[63] M. J. McDonnell, D. N. Stacey, and A. M. Steane. Laser linewidth effects in quantum state discrimination by electromagnetically induced transparency. *Phys. Rev. A*, 70(5):053802, Nov 2004. 3.3.1.2

[64] M. Shuker, O. Firstenberg, R. Pugatch, A. Ben-Kish, A. Ron, and Nir Davidson. Angular dependence of Dicke-narrowed electromagnetically induced transparency resonances. *Physical Review A*, 76(2):1–5, 2007. 3.3.2, 7.2

[65] A M Smith. Birefringence induced by bends and twists in single-mode optical fiber. *Appl. Opt.*, 19(15):2606–2611, August 1980. 3.3.2

[66] Jürgen Appel, Andrew MacRae, and Alexander I. Lvovsky. A versatile digital GHz phase lock for external cavity diode lasers. *Measurement Science and Technology*, 20(5):055302, May 2009. 3.4, 3.4

[67] D Hockel, M Scholz, and O Benson. A robust phase-locked diode laser system for EIT experiments in cesium. *Applied Physics B*, 94(3):429–435, 2009. 3.4, 3.4

[68] F. B. J. Buchkremer, R. Dumke, Ch. Buggle, G. Birkl, and W. Ertmer. Low-cost setup for generation of 3 GHz frequency difference phase-locked laser light. *Review of Scientific Instruments*, 71(9):3306, 2000. 3.4

[69] Paul Siddons, Charles S. Adams, Chang Ge, and Ifan G Hughes. Absolute absorption on rubidium D lines: comparison between theory and experiment. *Journal of Physics B: Atomic, Molecular and Optical Physics*, 41(15):155004, August 2008. 4.1, 4.3, 4.2.2

[70] R. Lang and K. Kobayashi. External optical feedback effects on semiconductor injection laser properties. *IEEE Journal of Quantum Electronics*, 16(3):347–355, March 1980. 4.1

[71] Ben E. Sherlock and Ifan G. Hughes. How weak is a weak probe in laser spectroscopy? *American Journal of Physics*, 77(2):111–115, 2009. 4.1

[72] E. Hecht. *Optics*. Addison-Wesley, 4th edition, 1998. 4.1

[73] Daniel A Steck. Rubidium 87 D Line Data. *URL http://steck.us/alkalidata/rubidium87numbers.pdf*, 2009. 4.2.2, 5.2.4

[74] Anthony E Siegman. *Lasers*. University Science Books, 1986. 1

[75] M. M. Hossain, S. Mitra, S. Chakrabarti, D. Bhattacharyya, B. Ray, and P. N. Ghosh. Study of width and height of EIT resonance in a Doppler broadened five-level system with varying probe power. *The European Physical Journal D - Atomic, Molecular, Optical and Plasma Physics*, 53:141–146, 2009. 10.1140/epjd/e2009-00108-7. 5.2.2

[76] RH Dicke. The Effect of Collisions upon the Doppler Width of Spectral Lines. *Physical Review*, 89(2):472–473, January 1953. 7.2, 1

[77] S. M. Iftiquar. Comment on“ Angular dependence of Dicke-narrowed electromagnetically induced transparency resonances”. 023813(2007):560012, November 2007. 7.2

[78] M Scherman, O S Mishina, P Lombardi, E Giacobino, and J Laurat. Enhancing electromagnetically-induced transparency in a multilevel broadened medium. *Optics Express*, 20(4):4346–51, February 2012. 8.1